EXPERIMENTAL FORCE COEFFICIENTS FOR A SHORT LENGTH SQUEEZE FILM DAMPER - EXPERIMENTAL FORCE COEFFICIENTS FOR A PLAIN JOURNAL BEARINGS -PRELIMINARY EXPERIMENTAL FORCE COEFFICIENTS FOR A FLEXTURE-PIVOT, 4 TILTING PADS JOURNAL BEARINGS (LBP)

MILLER ROBISON AND NICK WALTON

Dr. San Andres

May 1995

TRC-B&C-4-95

Texas A&M University
Mechanical Engineering Department

Experimental Force Coefficients for a Short Length Squeeze Film Damper.
Experimental Force Coefficients for a Plain Journal Bearing.
Preliminary Force Coefficients for a Flexure-Pivot, Tilting Pad Journal Bearing.

by

Miller Robison
Nick Walton
graduate research assistants

A Research Progress Report
to the
Turbomachinery Research Consortium

May 1995

TRC Project:
Test Rig for Identification of Rotordynamic Coefficients in Fluid Film Bearings.
Principal Investigator: Dr. Luis San Andres, Associate Professor

Table of Contents

ABSTRACT

This report describes the TRC generic fluid film bearing test rig and measurement procedure to identify the rotordynamic coefficients of generic fluid film bearings. The test apparatus allows exchange of test articles without modifications in the basic design of the machine. Impact load excitations bring the test articles into dynamic motion, and a frequency domain method identifies the stiffness, damping, and inertia force coefficients from an impedance matrix. Measurements for an open ended squeeze film damper at various journal center static (offset) positions are presented for dynamic tests with three levels of impact loads. In general, the identified damping coefficients correlate well with theoretical predictions. The stiffness and damping coefficients for a plain journal bearing are presented for rotor speeds of 1,800 and 3,600 rpm with varying static loads. The identified coefficients follow the same trends as theoretical values. A Flexurepivot™ tilt pad bearing donated by KMC, Inc., is currently undergoing investigation. Tests include mapping the static operating position and identifying the rotordynamic force coefficients at various static loads.

INTRODUCTION

Fluid film bearing elements play an integral role in the field of turbomachinery and rotordynamics. These elements support rotating shafts, help suppress vibrations, and also serve as high pressure seals. Fluid film bearing elements include squeeze film dampers, journal bearings, labyrinth seals, and tilting pad bearings, among others. The force coefficients of these fluid film bearings are known to affect turbomachinery dynamic performance and stability. Henceforth, accurate identification and prediction of force coefficients forms the base for sound mechanical designs.

The test rig used in this research provides turbomachinery design engineers with experimentally identified values of stiffness, damping, and inertia force coefficients of fluid film bearings. These experimental values serve to validate models or analyses used to predict bearing rotordynamic force coefficients.

After the test rig was designed and built in 1993, the inertia and damping force coefficients of an off-centered, open-ends squeeze film damper were identified. The test rig was revamped and the load vs. journal eccentricity, and the stiffness and damping force coefficients of a plain cylindrical journal bearing were identified. A flexure-pivot tilting pad bearing, donated by KMC, Inc., is currently under investigation. The experiments include mapping the static operating characteristics and identifying the stiffness and damping rotordynamic force coefficients of this novel bearing geometry.

Squeeze film dampers (SFD's) offer the unique advantages of vibrational energy dissipation, structural component load isolation, and stability promotion in inherently unstable rotor-bearing systems. SFD's provide damping forces along with substantial fluid film inertia forces to aircraft turbine engines. Design engineers need accurate values of damping and

inertia coefficients to produce sound designs. Poorly designed SFD's may cause highly non-linear rotor responses accompanied by jump-phenomena. Past investigations have shown that the force response of actual SFD's is difficult to predict. In general, experimental results for SFD forces and force coefficients demonstrate poor to average correlation with theoretical predictions based on classical lubrication theory (San Andres, 1995).

Critical rotating machinery uses plain cylindrical journal bearings for support and availability of damping forces. A properly designed journal bearing will not wear out while operating because a thin oil film supports the rotor. The theory that describes plain journal bearing operation does an adequate job of predicting the rotordynamic force coefficients (Childs, 1993). This fact makes the plain journal bearing an ideal fluid film bearing element to benchmark the operation of the test apparatus.

EXPERIMENTAL FACILITY

Figure 1 shows a cutaway view of the test rig. A static loader system and DC drive motor and pulley (not shown) also form part of the test apparatus. The peripheral systems consist of the data acquisition and computer system, and the support and test bearing lubrication systems. The support base is a steel block weighing 104 kg (230 lb), holding three high precision angular contact ball bearings. The test journal is mounted at the upper end of the shaft and may be interchanged depending upon the test bearing configurations. A belt and pulley connect the lower end of the shaft to a drive motor. A 7.5 kWatt (10 hp) DC motor drives the test rig with a top speed of 9,000 rpm. The first natural frequency of the shaft-support bearing and journal

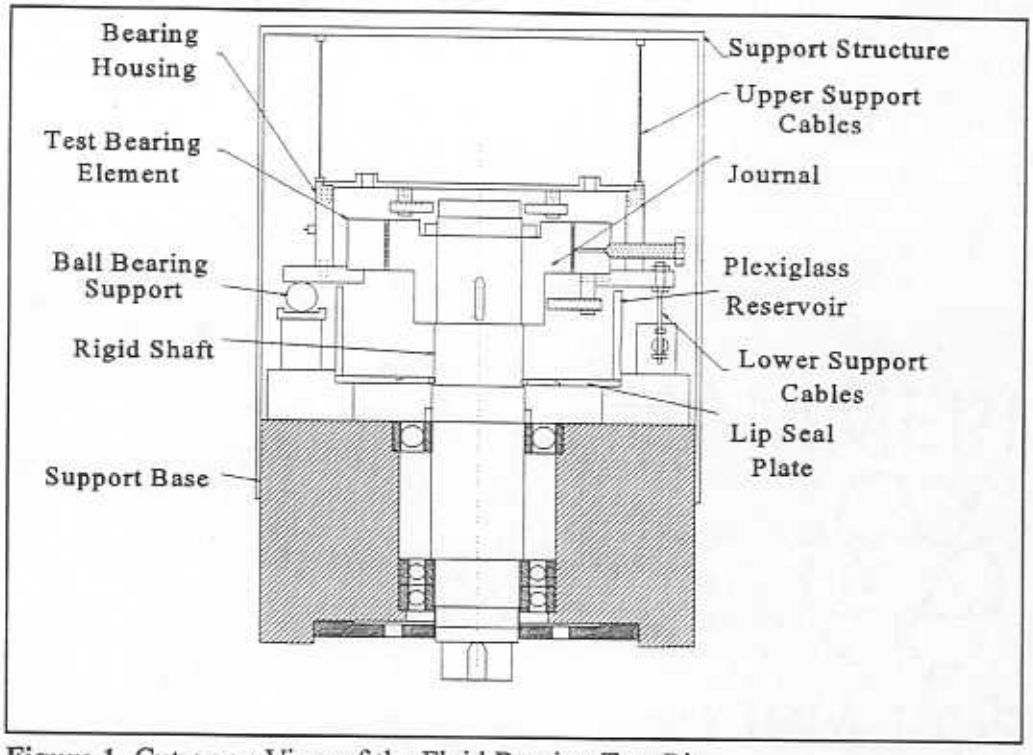

Figure 1. Cut-away View of the Fluid Bearing Test Rig

configuration equals 417 Hz. The maximum mechanical and electrical run-out equals 0.025 mm (1 mil) at the top of the shaft.

The test section hangs above the support base (see Fig.1). Four steel cables suspend the test housing, while three other cables hold it from below. The bottom steel wires serve as an axial load support mechanism to balance the thrust forces produced by the lubricant inlet pressure inside the test housing. The steel wires exhibit very low radial stiffness and negligible damping. The support system (cables, housing, and test bearing) natural frequency equals approximately 5 Hz. This support also prevents undesirable pitching motions of the test housing as past experiences demonstrate (Childs and Hale, 1993, Nordmann and Schöllhorn, 1980). Stainless steel balls located directly underneath the test housing hold the housing level during the exchange of various test components, and also provide a safety

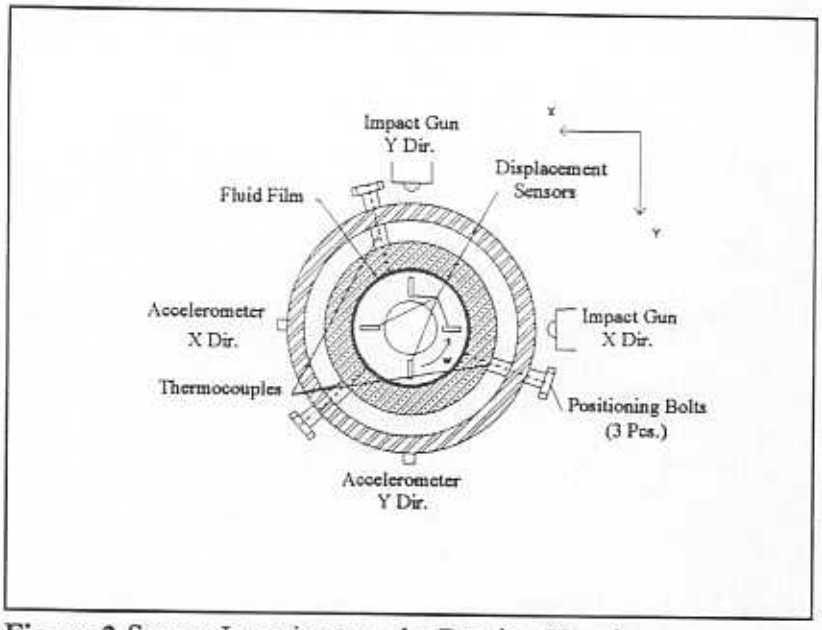

Figure 2 Sensor Locations on the Bearing Housing

restraint in case of cable failure during testing.

Three positioning screws hold the test bearing within the test housing. This housing also contains the displacement sensors and accelerometers needed to acquire the test bearing dynamic response. Figure 2 shows a schematic view of the sensor positions.

The fluid film lubrication system includes a high pressure (3.45 MPa [500 psi]), high flow (95 liter/min. [25 gal/min]) gear pump and an external reservoir that holds 144 liters (38 gal) of lubricant. A plexiglass reservoir catches the fluid after it has flowed through the test bearing. A metal plate with a lip seal keeps the lubricant used for the test fluid film bearing separate from the oil that lubricates the angular contact support bearings. The test bearing element dimensions should be within minimum and maximum allowable dimensions. Table 1 lists the permissible dimensions for various journals and fluid film elements.

A spring with a low stiffness of 315 kN/m (1,800 lb/in)

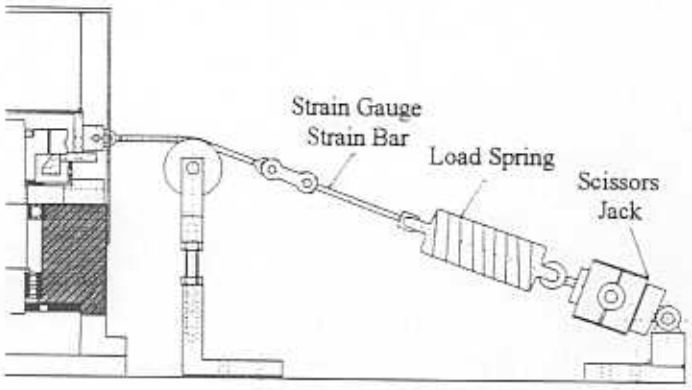

Figure 3: Static Loading Mechanism.

transmits a static load to create a bearing eccentricity, as shown in Figure 3. A scissors jack gives the desired deflection to the spring while a calibrated strain-gauge load cell measures the output force. A yoke/cable connection connects the static loader to the test housing. The support structure holds the displacement sensor and accelerometer data signal lines, along with the main oil lines carrying the lubricant into the test housing.

The upper cables attach to the support structure. Two orthogonally positioned impact guns bolt directly to the support base and strike the test housing. Calibrated impact loads range from 445 to 2,225 N (100 to 500 lb) and last approximately 0.7 msec.

Table 1. Permissible Dimensions and Operating Conditions

	Element Diameter	Journal Diameter	Element length	Radial Clearance
current	17.8 cm	12.7 cm	4.6 cm	0.155 mm
maximum	17.8 cm	15.9 cm *	4.6 cm	variable
minimum	16.0 cm	9.1 cm	N/A	N/A
Maximum Static Loads 4,450 N	Maximum Operating Speed 9,000 rpm	Available Fluid Supply Pressure 689 kPa	Drive Motor Power 7.5 kW	Sampling Frequency 12 kHz

* with length < 3.8 cm N/A - non-applicable

PARAMETER IDENTIFICATION PROCEDURE

The primary objective of the test apparatus is the identification of rotordynamic force coefficients of generic fluid film bearings. The parameter identification method transforms the measured bearing element time response to the frequency domain and extracts dynamic force coefficients from the bearing impedance matrix as a function of frequency. Cross-spectral density correlations reduce noise contamination and give an indication of the certainty of the results (Rouvas, Murphy, and Hale, 1992).

The model assumes the shaft and journal motion to be negligible, since its measured natural frequency is well above the operating range (~417 Hz). For small amplitude motions, the test housing dynamic equations are:

$$\begin{pmatrix} F_x - M_h\ddot{X} \\ F_y - M_h\ddot{Y} \end{pmatrix} = \begin{pmatrix} K_{xx}+K_c & K_{xy} \\ K_{yx} & K_{yy}+K_c \end{pmatrix} \begin{pmatrix} X \\ Y \end{pmatrix} + \begin{pmatrix} C_{xx}+C_c & C_{xy} \\ C_{yx} & C_{yy}+C_c \end{pmatrix} \begin{pmatrix} \dot{X} \\ \dot{Y} \end{pmatrix} + \begin{pmatrix} M_{xx} & M_{xy} \\ M_{yx} & M_{yy} \end{pmatrix} \begin{pmatrix} \ddot{X} \\ \ddot{Y} \end{pmatrix} \qquad (1)$$

where (X,Y) and their time derivatives denote the displacement, velocity, and acceleration components of the test bearing housing about an equilibrium position (see Fig. 2 for a descriptive view of the coordinate system used). F_x and F_y are the external forces applied to the test element, and the sets $\{K_{ij}\}$, $\{C_{ij}\}$, and $\{M_{ij}\}$, i,j=x,y, correspond to the fluid film bearing stiffness, damping, and inertia force coefficients. The support stiffness (K_c) and damping (C_c) are identified through rap tests performed on the housing without any lubricant present. The housing mass (M_h), which also includes the mass of the fluid contained inside the housing, is measured with a scale prior to testing. Preliminary tests show the housing and its cable support to be well represented by an uncoupled linear system.

The equations of motion are transformed to the frequency domain to give:

$$\begin{pmatrix} f_x\ (\omega) - M_h\ A_x\ (\omega) \\ f_y\ (\omega) - M_h\ A_y\ (\omega) \end{pmatrix} = \begin{pmatrix} H_{xx}\ H_{xy} \\ H_{yx}\ H_{yy} \end{pmatrix} \begin{pmatrix} x\ (\omega) \\ y\ (\omega) \end{pmatrix} \tag{2}$$

where (f_x,f_y) , (x,y) and (A_x,A_y) represent the external forces, bearing displacements, and accelerations in the frequency domain, and:

$$\begin{aligned} H_{ij} &= (K_{ij} + K_c\delta_{ij} - \omega^2 M_{ij}) + i\omega\ (C_{ij} + C_c\delta_{ij}) \\ &= H_{ij}^{Re} + i\ H_{ij}^{Im} \\ \delta_{ij} &= 1 \quad i = j\ ; \\ \delta_{ij} &= 0 \quad i \neq j\ ; \quad i = \sqrt{-1} \end{aligned} \tag{3}$$

correspond to the impedance coefficients of the test bearing element.

Two independent force excitations (F_x and F_y) are required to fully determine the elements of the impedance matrix as given

by:

$$\begin{pmatrix} f_x(\omega) - M_h A_x(\omega) \\ 0 - M_h A_y(\omega) \end{pmatrix} = \begin{pmatrix} x_{fx} & y_{fx} \\ x_{fy} & y_{fy} \end{pmatrix} \begin{pmatrix} H_{xx} \\ H_{xy} \end{pmatrix} \tag{4a}$$

$$\begin{pmatrix} 0 - M_h A_x(\omega) \\ f_y(\omega) - M_h A_y(\omega) \end{pmatrix} = \begin{pmatrix} x_{fx} & y_{fx} \\ x_{fy} & y_{fy} \end{pmatrix} \begin{pmatrix} H_{yx} \\ H_{yy} \end{pmatrix} \tag{4b}$$

where x_{fy} denotes the bearing X-displacement frequency due to an external impact load in the Y direction and so forth. The left hand side of (4) accounts for the housing inertial forces subtracted from the excitation force. The real component of H_{ij} yields the bearing and support cable stiffness and inertia coefficients, whereas the imaginary component yields the damping coefficients of the system. A frequency range is selected over which to calculate the impedance elements, then a simple least square method is used to identify all force coefficients.

A data acquisition software system acquires the dynamic forced response of the test bearing to an impact load. Figure 4 provides a schematic view of the data acquisition system. The main tasks of the software are to calibrate the sequential and simultaneous analog-to-digital (A/D) data acquisition boards, manage the computer memory buffers, record static and steady state signals, calibrate the impact guns, and record the bearing dynamic forced response. The rate of data acquisition is 12,000 samples/sec. for each signal. Anti-aliasing filters clip off undesirable noise caused by electromagnetic disturbances. The data acquisition conducts and records sixteen to thirty-two impact tests in each direction. The parameter identification program brings the displacement, impact, and acceleration signals into the frequency domain, and averages the system

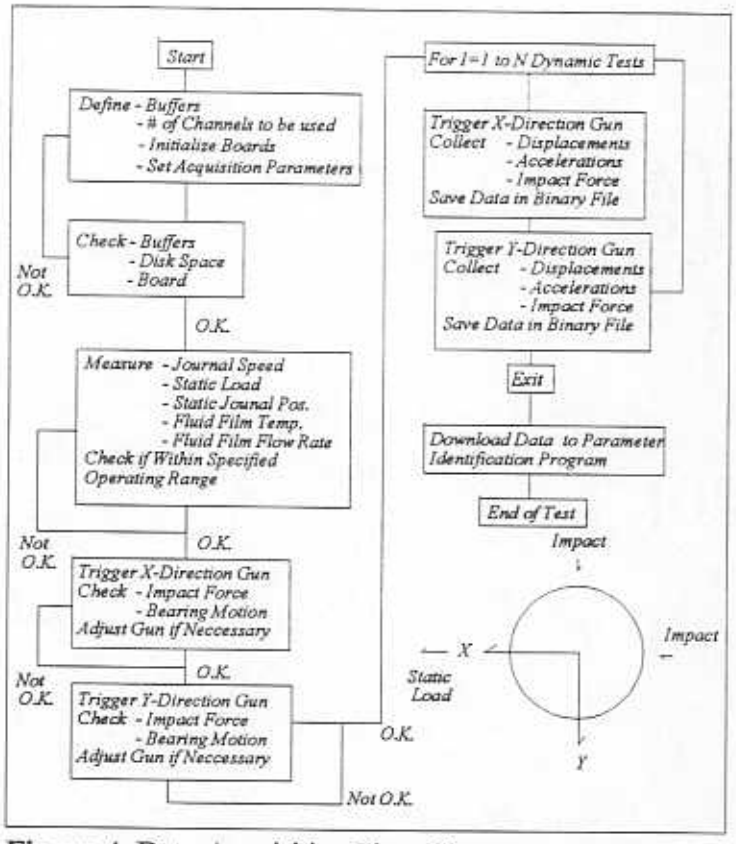

Figure 4. Data Acquisition Flow Chart

response in the two directions. The program uses a least squared error method to identify the coefficients over the requested frequency range.

I. EXPERIMENTAL FORCE COEFFICIENTS FOR A SHORT LENGTH SQUEEZE FILM DAMPER

SQUEEZE FILM DAMPER TEST PROCEDURE

The test rig apparatus described was slightly modified to perform experiments in a squeeze film damper mode. Four steel rods replaced the upper steel wire cables shown in Figure 1. The rods, with an overall radial stiffness of 385 kN/m (2,200 lb/in), increased the natural frequency of the dry housing to 30.4 Hz. The equivalent housing mass (M_h) including the lubricant equaled 10.56 kg. The test bearing has length L=4.57 cm, diameter D=12.7 cm, and nominal radial clearance c=0.127 mm. The static loader was not connected to the test housing during the SFD investigation. The tests consisted of statically off-centering the bearing housing relative to the journal by displacing the radial rods. Five configurations were obtained with static bearing offsets (in the X direction) ranging from -50% to 75% of the radial clearance. Negative static displacements denote proximity to the impact gun, while positive static displacements indicate otherwise. The oil used in the tests corresponds to an ISO VG 2 lubricant with a specific gravity of 0.796. The lubricant was heated to three temperatures equal to 21, 27 and 32°C with viscosities measured prior to tests, and equal to 0.0026, 0.0023, and 0.0021 Pa-sec, respectively. The experiments were performed with a pressure supply less than 34 kPa (5 psig) to warrant continuous flow of lubricant across the bearing element.

Impacts were delivered to the test housing in the X and Y directions. The largest amplitude of motion of the damper housing, given as a percentage of the radial clearance, was used to gauge the impact forces. In this manner, repeated tests with impact loads of approximately 440, 990, and 1,110 N (100, 200,

and 250 lb) enabled the test bearing to move with peak amplitudes equal to 10%, 20% and 30% of the film clearance. The impact loads required to achieve the desired dynamic journal displacements increased slightly with the static bearing offset. For the +75% offset configuration, a 30% impact was not used because this would have forced the housing and journal to collide.

All of the test results are compared with theoretical predictions based on earlier analysis for cavitated, finite length SFD's (San Andres and Vance, 1986). The analysis includes temporal fluid inertia effects in the flow equations. The viscous pressure (p_0) and the inertial pressure (p_1) are superimposed to determine the total squeeze film pressure ($p_0 + Re_s * p_1$). The differential equations for pressure in an off-centered journal SFD executing small amplitudes of motion at a known frequency are given by San Andres and Vance (1986) as:

$$\frac{\delta}{\delta\theta}\left(H^3 \frac{\delta \bar{p}_0}{\delta\theta} \right) + \frac{\delta}{\delta\xi}\left(H^3 \frac{\delta \bar{p}_0}{\delta\xi} \right) = 12 \frac{\delta H}{\delta\tau}$$

$$\frac{\delta}{\delta\theta}\left(H \frac{\delta \bar{p}_1}{\delta\theta} \right) + \frac{\delta}{\delta\xi}\left(H \frac{\delta \bar{p}_1}{\delta\xi} \right) = \alpha \frac{\delta^2 H}{\delta\tau^2} \qquad (5)$$

where (θ, ξ, τ) define the dimensionless circumferential, axial, and time coordinates, H is the instantaneous fluid film thickness, and p_0 and p_1 describe the viscous and inertial pressures, respectively. Re_s is defined as the squeeze film Reynolds number ($\rho\omega c^2/\mu$). α corresponds to an inertial wall shear stress($\alpha \approx 1.2$) coefficient for small amplitude, off centered journal motions. A finite difference method solved these flow equations for the pressure fields within the squeeze film lands. Integrating the calculated pressure fields over the surface of the damper journal provides the force coefficients.

An approximate solution (based on a correction factor applied to the long SFD model) was developed in conjunction with the above numerical analysis (San Andres and Vance, 1986). The force coefficients for finite length SFD's (M_{ij}, C_{ij}) with open ends are determined as the product of those coefficients for long SFD's ($M_{ij\infty}, C_{ij\infty}$) multiplied by a correction factor, Π.

$$\begin{aligned} M_{ij} &= M_{ij\infty}\,\Pi \\ C_{ij} &= C_{ij\infty}\,\Pi \end{aligned} \qquad i,j = x,y \tag{6}$$

The correction factor (Π) depends upon the L/D ratio and the SFD static eccentricity (e/c). A comparison between the finite difference method and the approximate analytical method showed that the two models were in very good agreement. Easiness of use is the advantage of the approximate method. Hence, the approximate method was selected to compare with the experimental damping and inertia force coefficients from the test bearing element.

The displacement, acceleration, force, and temperature transducers used in the test rig have uncertainties of ±2 μm, ±0.098 m/s^2, ±22 N, ±0.1° C, respectively. Individual measurement uncertainties are calculated using a standard method (Kline and McClintock, 1953). The overall uncertainty in the identified rotordynamic coefficients consists of individual deviations introduced by the data acquisition process, the least squared curve fitting method, the transducer uncertainties, and the parameter identification method. The uncertainties for nominal damping and inertia values of 9,366 N*sec/m and 2.9 kg equal 9% and 20%, respectively.

TEST RESULTS

Figure 5 depicts a typical time response (X,Y) of the open end SFD for an impact load in the Y direction. The test results correspond to a statically centered housing position with an impact load of 1,100 N lasting approximately 0.7 msec. The measurements show an overdamped system without cross-coupling effects. The small amplitude high frequencies shown in the displacements arise from inherent noise from the proximity sensors used. Figure 6 shows the real and imaginary parts of the test SFD impedance coefficients for impact excitation at the centered position for impact loads enabling large amplitude bearing motions. The imaginary part of the direct impedances (H_{XX}, H_{YY}) shows a linear behavior denoting the squeeze film damping contribution. This figure also illustrates the curve-fits as given from equation (3) and demonstrate the goodness of the theoretical model to represent the test data on the frequency range from 0 to 100 Hz. The cut-off frequency of 100 Hz provided the most reliable results. No indications of higher frequencies were observable in the test results. Note that the cross-coupled impedance elements (H_{XY} , H_{YX}) proved rather small and were within the bounds of the experimental uncertainty.

The averaged squeeze film damper force coefficients are extracted by curve fitting the discrete impedance curves obtained from each test. The direct damping (C_{XX}, C_{YY}) and inertia (M_{XX},M_{YY}) coefficients are shown in figures 7 through 10 as a function of the static journal eccentricity for all test conditions. The test results are presented in dimensionless form and compared to theoretical predictions based on earlier analysis (San Andres and Vance, 1986) for cavitated, finite length SFD's. Each figure contains the appropriate factor used to present the dimensionless coefficient. The measurements did not show any significant values of cross-coupled coefficients. The estimated

values of squeeze film stiffness coefficients (K_{xx}, K_{yy}) are relatively small (unimportant) and range from 9,150 N/m (52 lb/in) to -508,758 N/m (-2,905 lb/in).

The damping coefficients depicted in Figures 7 and 8 increase with the static offset journal position, but at a lower rate than the theoretical predictions. The dimensionless damping coefficient C_{YY} agrees well with theory, but there is a large scatter in the test data for the coefficient C_{XX}. Note that this coefficient is the one aligned with the static offset position (X direction). The direct damping coefficients are practically insensitive to the magnitude of the impact loads used, although these were large enough to move the test housing with amplitudes as large as 30% of the nominal film clearance. The experimentally estimated value of the damping coefficient C_{YY} at the centered position and at a fluid temperature of 21°C, is equal to 11,171 N-s/m (64 lb*s/in) for a 30% impact load.

The test direct inertia coefficients (M_{XX}, M_{YY}) depicted in Figures 9 and 10 , are larger than the analytical predictions for most tests performed. The predicted inertia force coefficients at the centered position and at a fluid temperature of 21°C, equals 4.66 kg, while most experimentally estimated values range from 5 to 11 kg. Note that the force coefficients are extracted from data over a narrow frequency range (0-100 Hz). The measurements show inertia force coefficients of important magnitude considering the small (L/D) ratio of the damper tested. These estimated values are consistent with the past investigations for SFD's (Ramli, Roberts, and Ellis, 1987).

CONCLUSIONS

Experimental damping and inertia force coefficients for a short length, open ends squeeze film damper are presented. Tests were conducted at various off-center journal positions, three

lubricant temperatures, and increasing levels of impacts resulting in bearing motions with amplitudes to 30% of the thin film clearance. Estimated damping coefficients agree well with theoretical predictions and do not show a significant variation with the magnitude of impacts used. Most test inertia force coefficients are larger than theoretical predictions and practically insensitive to the static offset position. The discrepancies with the theoretical values may be due to the test SFD not showing the extent of cavitation region that theory assumes. Cross-coupled force effects are determined to be negligible for all test configurations.

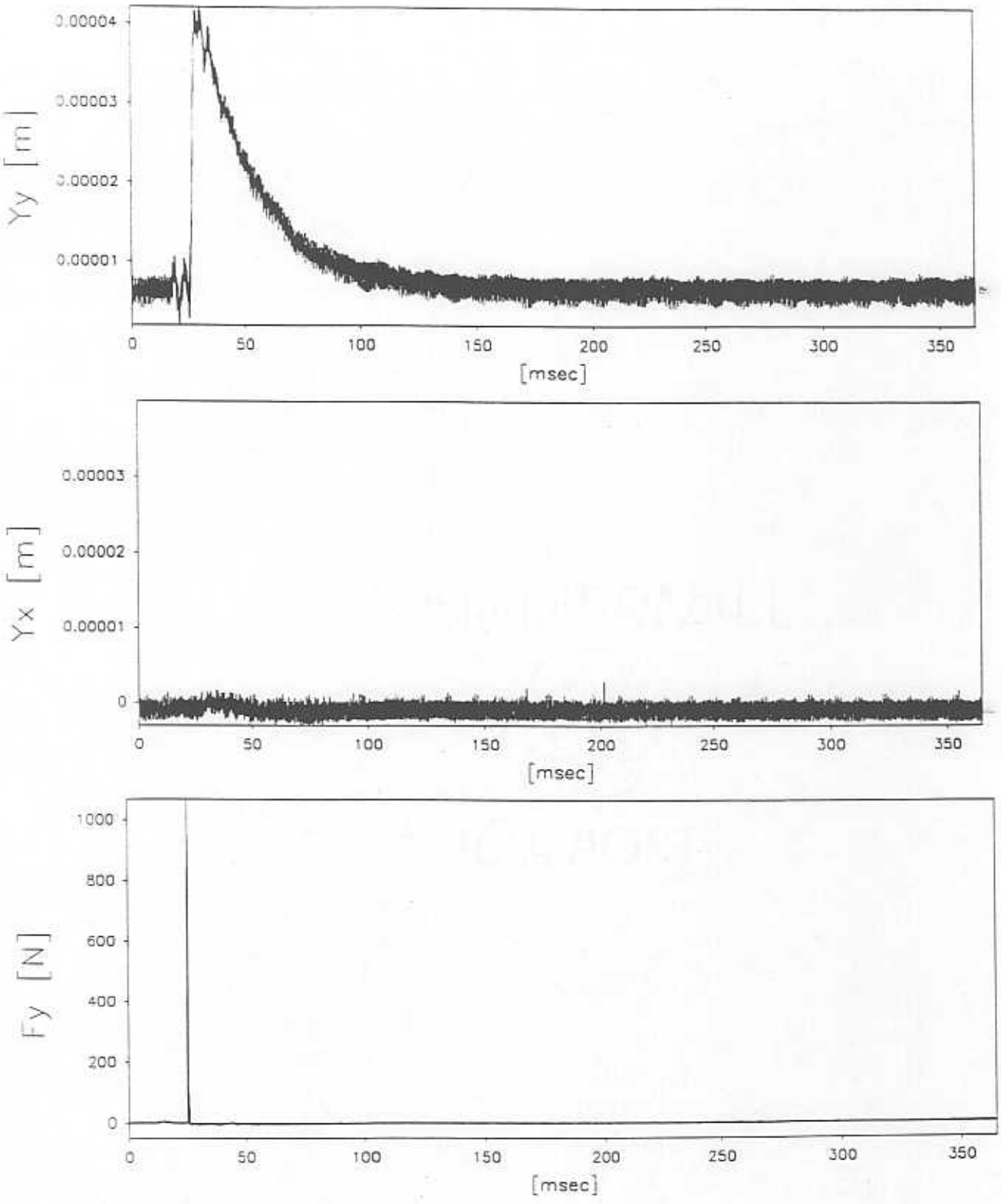

Figure 5. Time Response from a 30% Impact (Fy) at Centered Position, Fluid Temp. 32° C

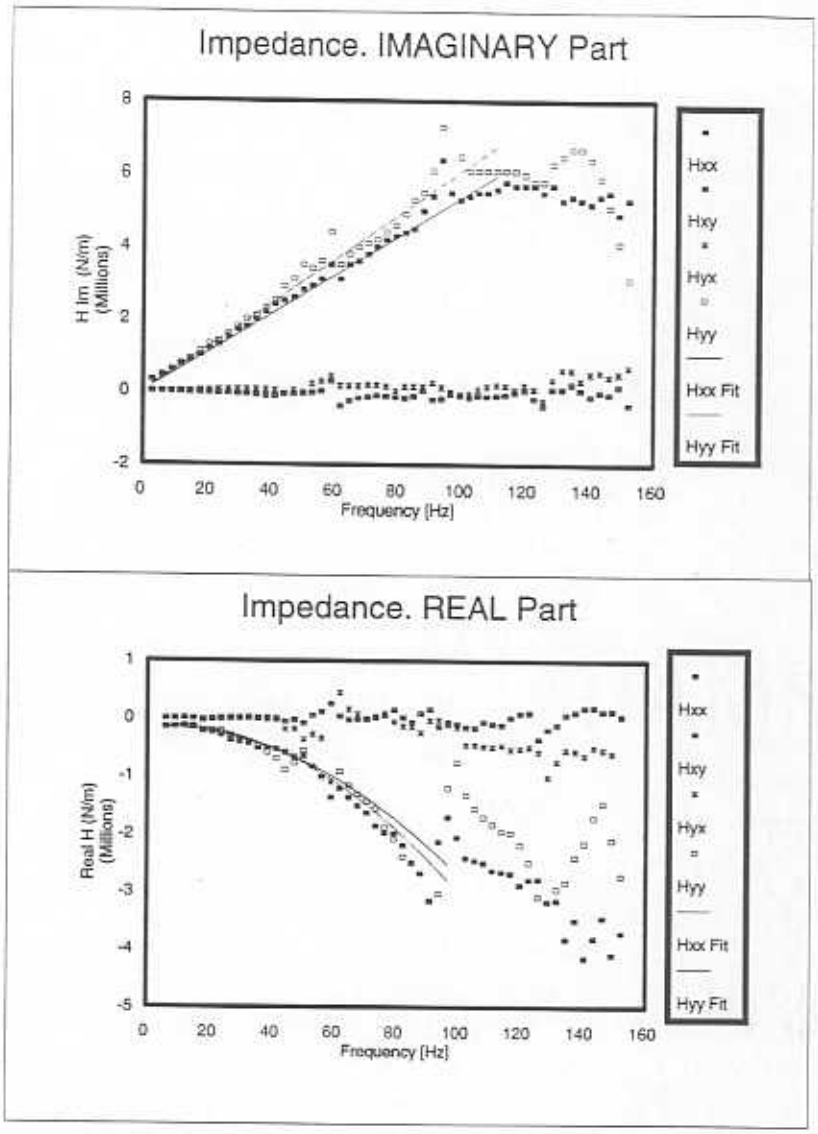

FIGURE 6. TYPICAL AVERAGED IMPEDANCES AT THE CENTERED POSITION, 27 DEG. C, AND 20% IMPACT LOADS

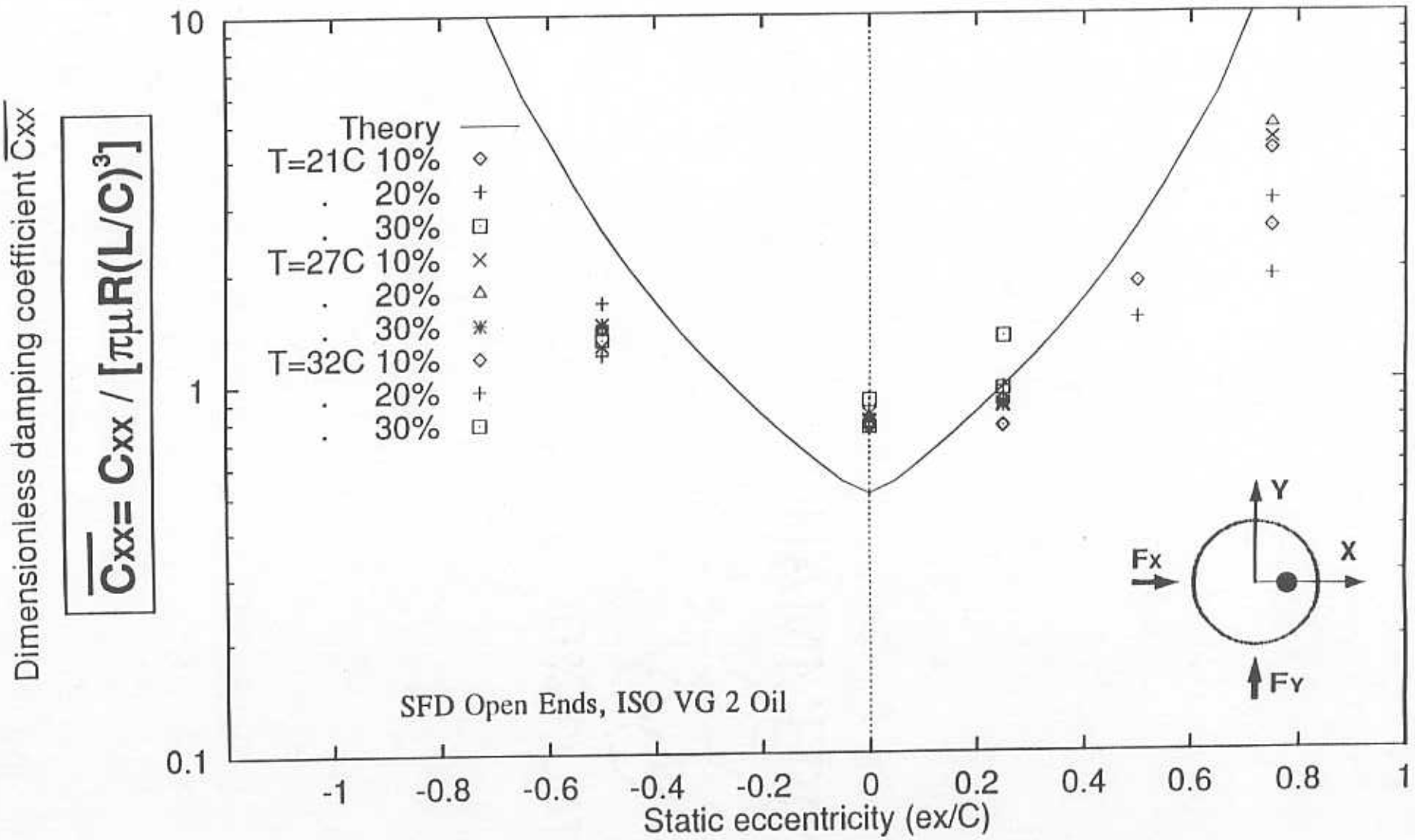

Figure 7. Dimensionless Experimental and Theoretical Direct Damping Coefficient $\overline{Cxx}$ vs. Static Eccentricity. Fluid film temperature and magnitude of impact vary.

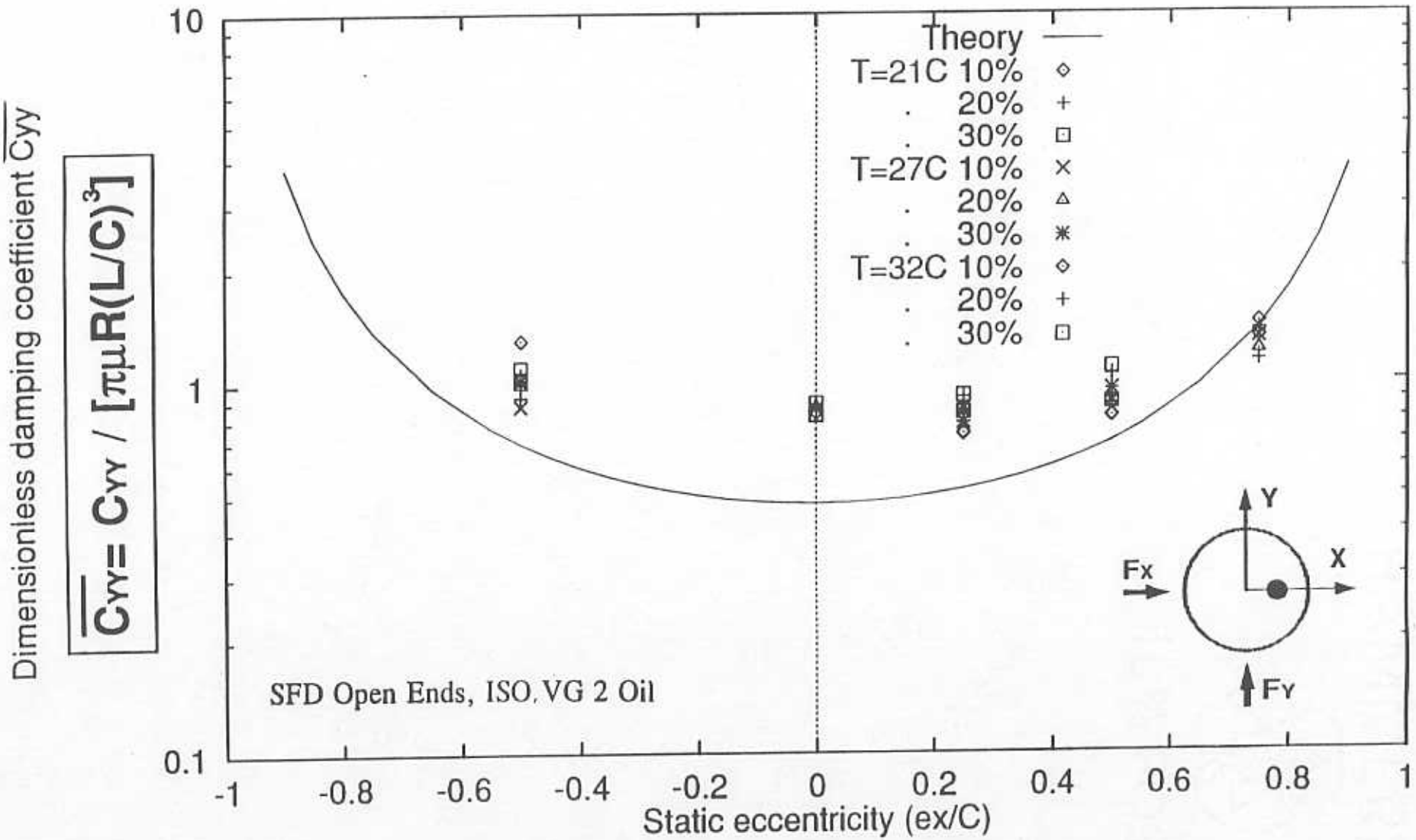

Figure 8. Dimensionless Experimental and Theoretical Direct Damping Coefficient $\overline{Cyy}$ vs. Static Eccentricity. Fluid film temperature and magnitude of impact vary.

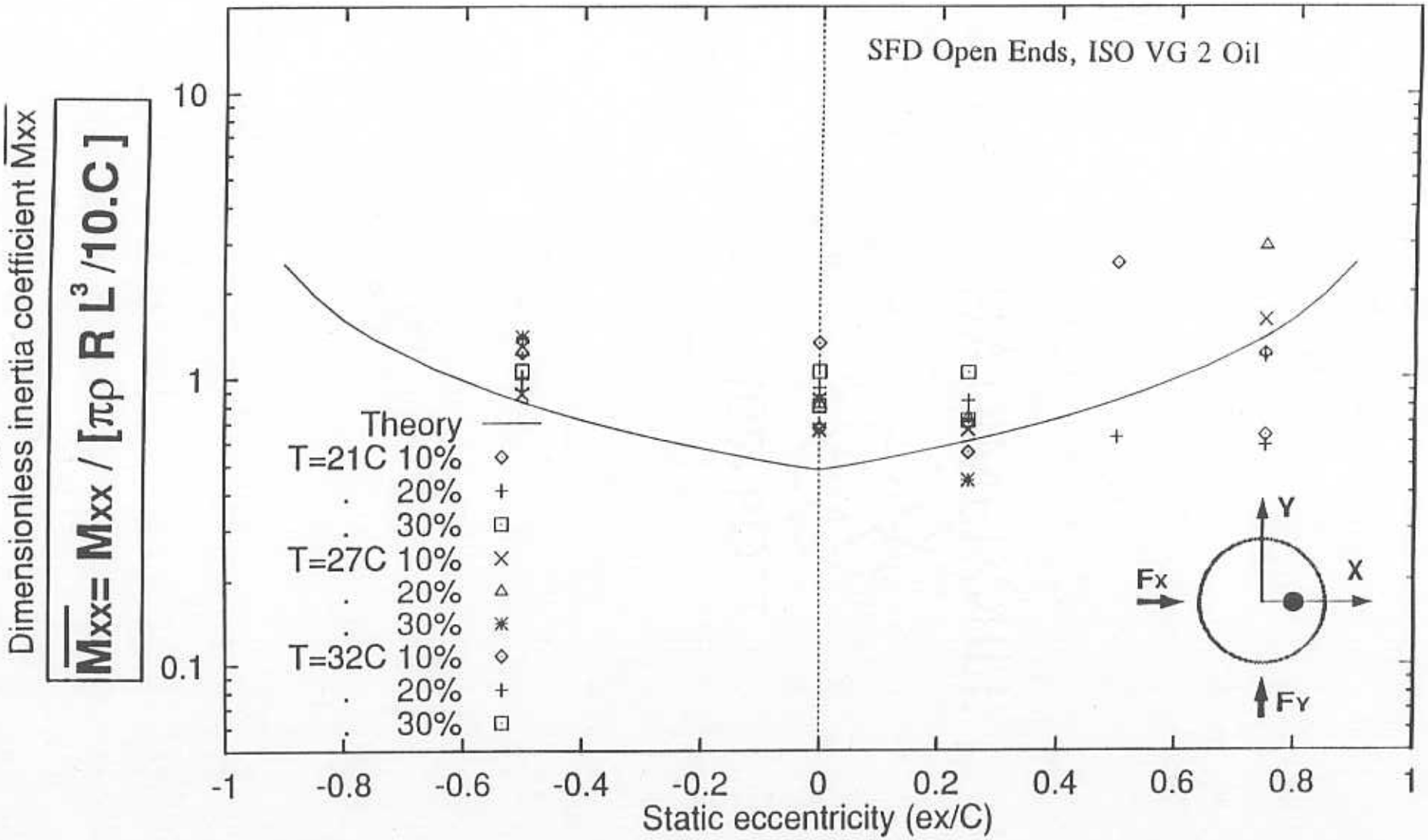

Figure 9. Dimensionless Experimental and Theoretical Direct Inertia Coefficient $\overline{Mxx}$ vs. Static Eccentricity. Fluid film temperature and magnitude of impact vary.

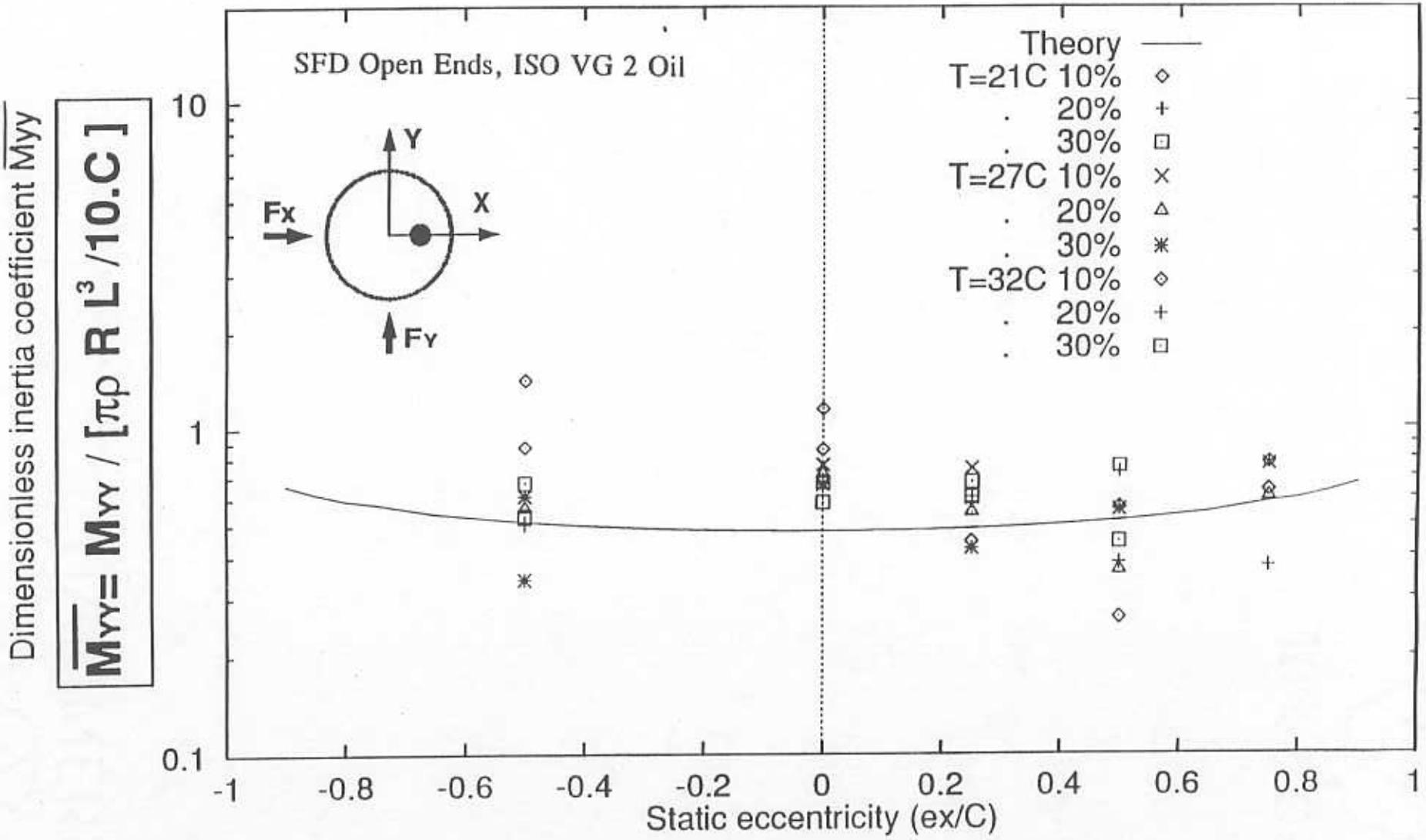

Figure 10. Dimensionless Experimental and Theoretical Direct Inertia Coefficient $\overline{Myy}$ vs. Static Eccentricity. Fluid film temperature and magnitude of impact vary.

II. EXPERIMENTAL FORCE COEFFICIENTS FOR A PLAIN JOURNAL BEARING

PLAIN JOURNAL BEARING TEST PROCEDURE

The steel bars used in the SFD investigation were replaced with the original cable support system described earlier. The plain cylindrical journal bearing tested had a length L=36.89 cm, diameter D=12.7 cm, and a nominal radial clearance of c=142 μm at room temperature.

Tests were performed at speeds of 1,800 rpm and 3,600 rpm. At each speed, the bearing element underwent a series of static loads ranging from 220 Newtons to 1,780 Newtons, by increments of 220 Newtons. The static operating conditions were recorded at each load, when a state of thermal equilibrium was reached.

The measured static operating conditions included the static load, fluid film temperature, speed, bearing journal position, and their respective standard deviations. The oil used in both tests was an ISO VG 22 lubricant with a specific gravity of 0.857. The film temperature was monitored throughout each investigation by a thermocouple located near the converging wedge of the journal bearing. The film temperature at each static load was measured, and an average of these values for each test speed was calculated. The average recorded oil film temperature and viscosity were 36.2 °C and 0.0201 Pa-sec during the 1,800 rpm test, and 47.5 °C and 0.0123 Pa-sec during the 3,600 rpm test. The oil inlet pressure was approximately 110 kPa (16 psi). This feed pressure assured positive flow across the bearing film land. Thirty-two impacts excited the test housing in the X and Y directions at each static load condition. The impact load magnitudes were on the order of 4,000 N and lasted approximately 0.7 msec.

All of the test results were compared to theoretical predictions obtained from an isothermal, isoviscous finite

element program entitled PADFEM (San Andres, 1994). This computational program solves the Reynolds equation for inertialess, isoviscous, and isothermal laminar flows (Pinkus and Sternlicht, 1961):

$$\frac{\delta}{\delta x}\left(\frac{H^3}{12\mu}\frac{\delta P}{\delta x}\right) + \frac{\delta}{\delta y}\left(\frac{H^3}{12\mu}\frac{\delta P}{\delta y}\right) = \frac{\Omega R}{2}\frac{\delta H}{\delta x} + \frac{\delta H}{\delta t} \qquad (7)$$

where (x,y) are the bearing plane circumferential and axial coordinates, H is the fluid film thickness, P is the fluid film pressure, μ is the fluid viscosity, Ω is the journal speed, and R is the journal radius. The static and dynamic pressure fields generated for an eccentric journal executing small amplitude motions about an equilibrium position are known as the zeroth-order and the first-order pressure fields, respectively. A mathematical perturbation analysis is used to derive the differential equations that define these pressure fields. The bearing forces are found by integrating the calculated pressure fields over the journal surface. The perturbed forces determine the rotordynamic stiffness and damping force coefficients.

TEST RESULTS

Figure 11 shows a typical time response of the plain journal bearing operating at 3,600 rpm, during an impact loading of 3,200 N, and for an applied load equal to 220 N. This figure demonstrates the presence of cross-coupling in a plain journal bearing, because the X-direction impact causes motion and acceleration in the Y direction. Notice how quickly the bearing response to the impact loading dies out. After three journal revolutions, the transient response dies out completely. The transient dies out after one bearing revolution at higher static loads. The shaft runout signature in Figure 11 is identified as

the periodic wave starting at 115 msec. and continuing to the end of the X and Y bearing position time response. An attempt to reduce the runout by manually sanding the shaft did not produce favorable results. Instead of getting a large runout with one frequency, a large runout with four harmonics was produced.

Figure 12 shows the real part of the 32 impact averaged, direct and cross-coupled journal bearing impedances, while figure 13 shows the imaginary part of the direct and cross-coupled journal bearing impedances. The static load equals 900 N and the operating speed is 3,600 rpm. The straight lines in the figures represent the identified rotordynamic coefficients. The damping coefficients arise from the slope of the imaginary part of the impedances, as shown earlier in the squeeze film damper investigation. The stiffness coefficients are identified as the horizontal components of the real impedances. The effects of fluid inertia in a plain journal bearing are usually negligible. However, the presence of fluid inertia causes a downward curvature in the real part of the impedances, as in the case of the SFD tested earlier. In Figure 12, the downward curvature at the higher frequencies is caused by the synchronous, or running speed component at 60 Hz. The small spike located at 30 Hz in Figures 12 and 13 show the influence of the subsynchronous response (i.e. system natural frequency).

The cut-off frequency for parameter identification was just below the operating speed of the test bearing, i.e. 26 Hz and 55 Hz for the 1,800 rpm and 3,600 rpm tests, respectively. The running speed frequency component in the impedances was polluted with shaft runout and could not be used in the parameter identification program. Even though the cut-off frequency was below the running speed, its influence extended beyond the cut-off and forced the immediately surrounding amplitudes to drop.

Accurate location of the bearing center proved to be

difficult because the static bearing center was markedly different from the running bearing center. The bearing center was approximately located by completely unloading the bearing at test speed. Care was taken when the bearing was operating in the unloaded state because the bearing would go unstable if slightly disturbed. The force due to the oil feed pressure helped stabilize the bearing if whirling started.

Figure 14 shows the X and Y journal eccentricity components at the applied static loads along the X-direction for operation at 1,800 rpm. Theory underpredicts the Y-journal center displacement and slightly overpredicts the X eccentricity. Figure 15 shows similar results for speeds at 3,600 rpm. The clearance used for the calculation of the eccentricity is measured upon completion of the tests, before the test rig cools down. Figure 16 presents the total bearing eccentricity at both test speeds. The error bars represent the journal position standard deviation caused by electrical and mechanical runout. At 3,600 rpm the test bearing underwent loading and unloading. At 1,800 rpm, the test bearing experienced an increasing loading cycle only. Figure 17 presents the eccentricity at both test speeds compared to the short-bearing Sommerfeld number, i.e. (Lund, 1966)

$$S = \frac{\mu NLD}{4W}\left(\frac{L}{c}\right)^2 \tag{8}$$

Where μ is the fluid viscosity, L is the bearing length, N is speed in revolutions per second, D is the bearing diameter, W is the applied static load, and c is the bearing measured radial clearance. This equation is valid for bearings with an L/D ratio less than, or equal to 0.20. The bearing under investigation has an L/D ratio of 0.30. The experimental results do not compare

well with the theoretical predictions.

The drag torque produced by the test bearing could not be correctly measured. A special torque measuring device identified the drag torque by measuring the deflection of a spring that opposed test housing rotation. The stiffness coefficient of this spring was much too high, and the measured deflections were too small to accurately determine the moment that counteracted the drag torque.

Figures 18 and 19 present the direct (Kxx, Kyy) and cross-coupled (Kxy, Kyx) stiffness coefficients at each load condition for the 1,800 rpm tests. The experiments follow the same trend as theoretical values given by the continuous lines; however, the predictions overestimate the stiffness coefficients in all cases.

Figure 20 shows the direct (Cxx, Cyy) damping coefficients at each static load for 1,800 rpm. The experimental direct damping coefficients also follow the same trends as the theoretical values. The theoretical results overpredict the Cxx coefficients and underpredict the Cyy coefficients. The cross-coupled damping coefficients (Cxy, Cyx) presented in Figure 21 compare better with theoretical predictions, but contain a large amount of scatter. Note that the Kyy, Kyx, Cyy, and Cyx force coefficients are not presented for the unloading cases at 3,600 rpm since a loose connection in the Y-direction impact gun produced faulty results.

Figure 22 shows the direct (Kxx, Kyy) stiffness coefficients at 3,600 rpm. The theoretical values overestimate the Kxx stiffness coefficients, as in the tests at 1,800 rpm. The Kyy stiffness coefficients follow the theoretical predictions. Figure 23 presents the cross-coupled (Kxy, Kyx) stiffness coefficients at 3,600 rpm. Both the Kxy and Kyx stiffness coefficients follow theoretical predictions, with the theory producing slightly higher values. Figure 24 presents the direct

(Cxx, Cyy) damping coefficients at 3,600 rpm. Again, theoretical values overestimate the Cxx damping coefficients and underestimate the Cyy coefficients. The cross-coupled damping coefficients presented in Figure 25 show a large scatter.

Figures 26 and 27 present the whirl frequency ratio and the equivalent stiffness of the plain journal bearing at both testing speeds. The whirl frequency ratio and the equivalent stiffness values compare poorly with theory. This poor comparison reduces the confidence in the experimentally obtained rotordynamic force coefficients.

A test was performed on the parameter identification program to check the averaging method used by the program and to generate the standard deviations of the identified force coefficients. Figures 28 and 29 show some results from this test. Thirty-two impacts were delivered to the test bearing at each load condition. The force coefficients were identified in turn using 4, 8, 16, to 32 impact trials. The standard deviation generated with this method applies only to the tests performed on the plain journal bearing with an applied load of 900 N and at a running speed of 3,600 rpm. The standard deviations are as follows: 230 kN/m for Kxx; 770 kN/m for Kyy; 760 kN/m for Kxy; 370 kN/m for Kyx; 3 kN*s/m for Cxx; 2 kN*s/m for Cyy; 1 kN*s/m for Cxy; and 3 kN*s/m for Cyx.

CONCLUSIONS AND RECOMMENDATIONS

Experimental stiffness and damping force coefficients for a plain cylindrical journal bearing are presented. Tests were conducted at various statically applied loads and operating speeds of 1,800 and 3,600 rpm. The identified force coefficients follow the same trends as theoretical predictions, but compare poorly.

Note that the theoretical predictions do not take into

account thermal effects on the journal bearing performance. This could partially account for the discrepancy between the measured and the predicted journal center operating position. This discrepancy may be mostly attributed to localized thermal distortion in the brass bearing.

There are many possible reasons why the rotordynamic force coefficient identification tests did not provide good results. The theoretical model bases its rotordynamic force coefficient calculations on its predicted journal center static operating position. The measured static operating positions do not match well the predicted values. This leads to the first error source. The large discrepancies can also be attributed to the effects of the static loading mechanism. The load spring has a stiffness of 315 kN/m (1,800 lbf/in), and is mounted in parallel with the journal bearing. The loader stiffness could be tainting the Kxx, Kxy, Cxx, Cxy coefficients because of the X-direction orientation. Friction in the loading mechanism may also restrict the housing motion in the X-direction.

The impact guns are the weakest component in the TRC generic fluid film bearing test rig. Many problems have arisen while testing and cause much data to be rejected. These problems include electrical connections that loosen, double impacts caused by a weak recoil spring, loose hammer tips, and broken mounting tabs.

Another problem stems from the cross-spectral density method. This method reduces the effects of noise with frequency domain techniques that implement sinusoidal excitations (Childs and Hale, 1993). This method does not work well with impact excitations. The cross-spectral density method compares the Fourier transform of the impact signal to the Fourier transform of the response signals. Any response frequencies that do not match with frequencies contained in the impact signal are

rejected. The Fourier transform of an ideal impact signal is a slowly decaying line composed of all frequencies that tapers off at very high frequencies. The cross-spectral density method will not reject any synchronous or supersynchronous frequency responses caused by shaft runout or noise, because these unwanted frequencies are also included in the impact frequency response.

Recommendations for further enhancement of the TRC generic fluid film bearing test rig are numerous. Needed changes on the data acquisition system include the ability to automatically detect double impacts, faulty connections, or noisy connections emanating from the impact guns. The measurement of the journal bearing static operating position would be more accurate if all four displacement sensors were used during static data acquisition. The final modification to the data acquisition system entails measuring static data with DC coupling and dynamic data with AC coupling. A DC offset in the dynamic signals creates a 0 Hz bias in all the bearing impedances. This 0 Hz component can be removed from the bearing impedances if AC coupling were used during dynamic data acquisition.

The acquisition of several items will also enhance the TRC generic fluid film bearing test rig. A new static loader spring with no pre-load and a stiffness coefficient of 140.1 kN/m (800 lbf/in) might reduce the load spring's effects on the X-direction force coefficients. Two shakers to replace the impact guns would increase the accuracy and confidence of the identified rotordynamic force coefficients extracted from the test apparatus. The response of the plain journal bearing to impact excitations was not large enough compared to the mechanical and electrical runout. In every impact test, the transient response of the bearing dies out within three journal revolutions. Shakers would provide a much improved bearing excitation with longer duration.

The TRC generic fluid film bearing test rig generated good results for the squeeze film damper investigation; however, the results for the plain journal bearing were poor. The previously listed changes to the test rig and purchases can only enhance the quality of results produced on the test apparatus.

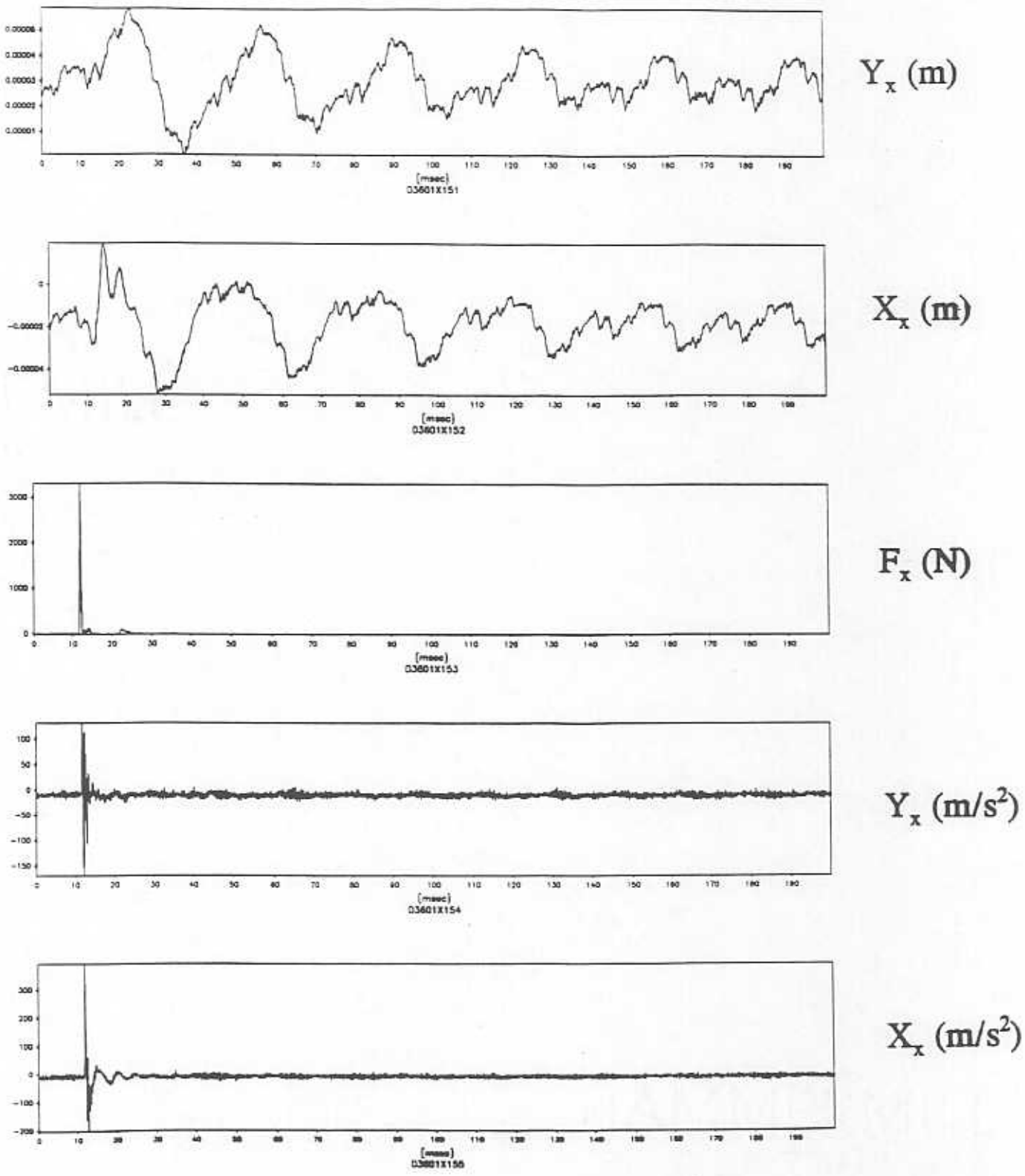

Figure 11. Bearing Time Response from a 3,200 N Impact (Fx) at a Static Load of 220 N and an Operating Speed of 3,600 rpm.

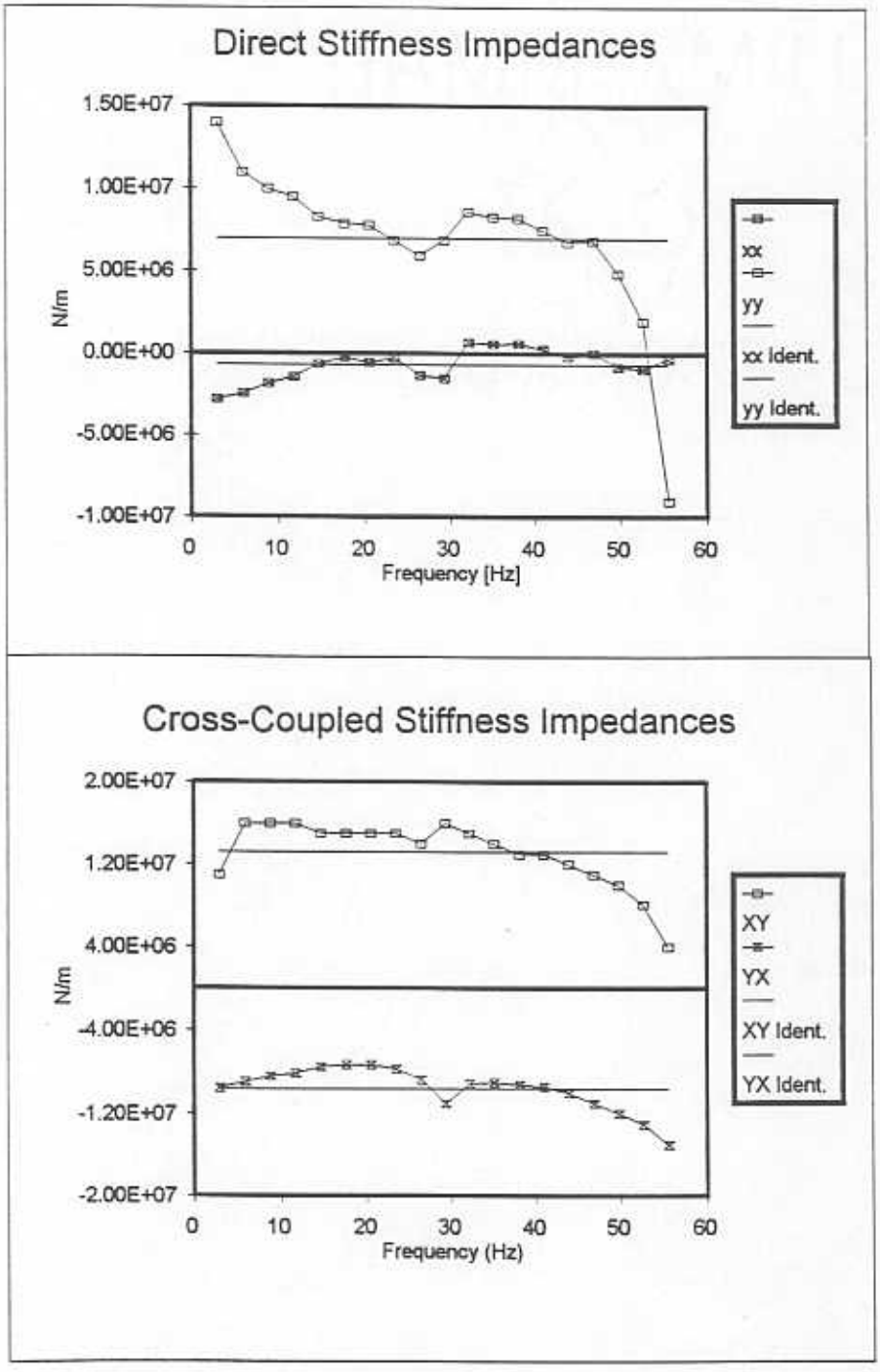

Figure 12. Typical Averaged Real Impedances for the Plain Journal Bearing with a 900 N Static Load, at 3,600 rpm.

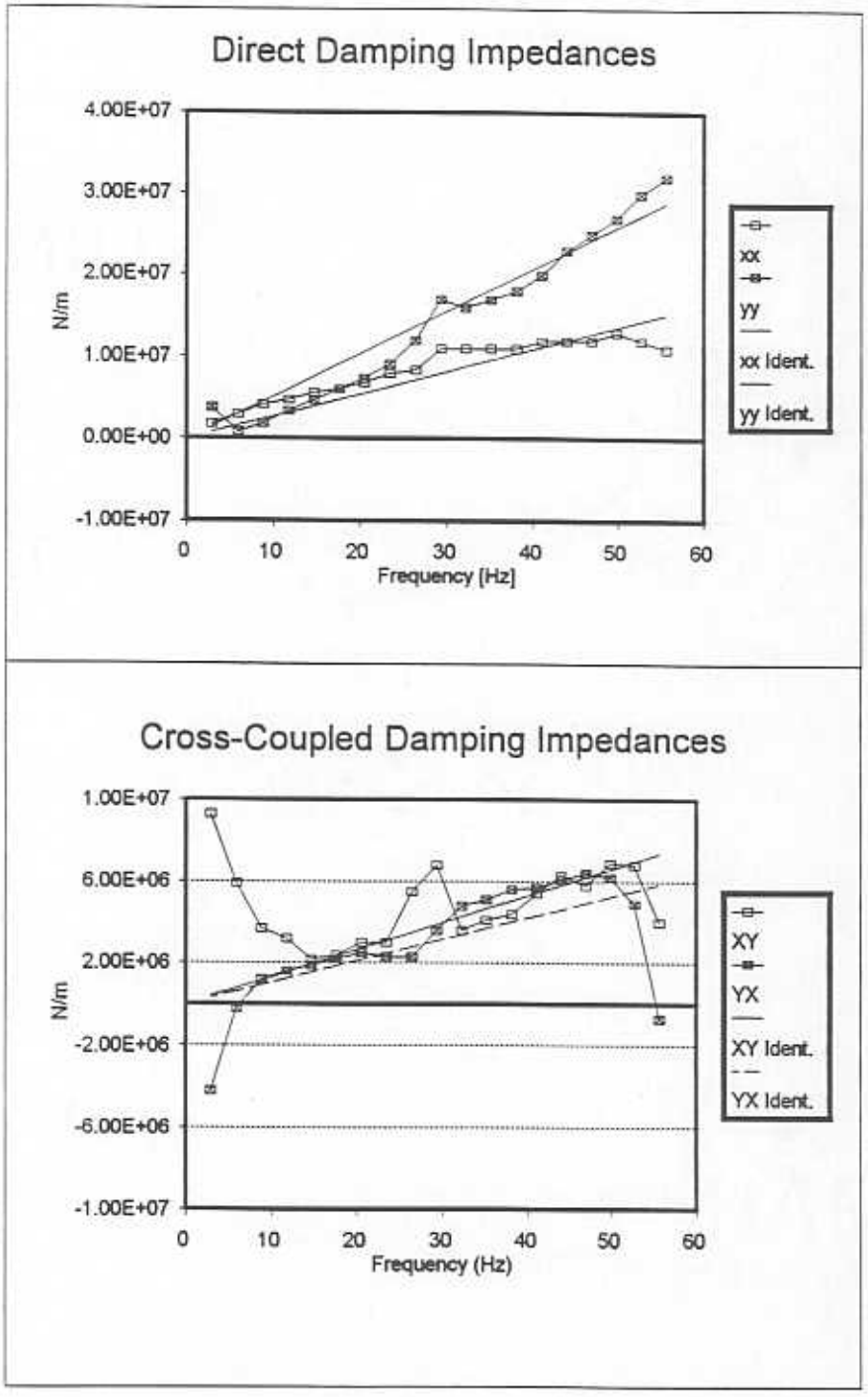

Figure 13. Typical Averaged Imaginary Impedances for the Plain Journal Bearing with a 900 N Static Load, at 3,600 rpm.

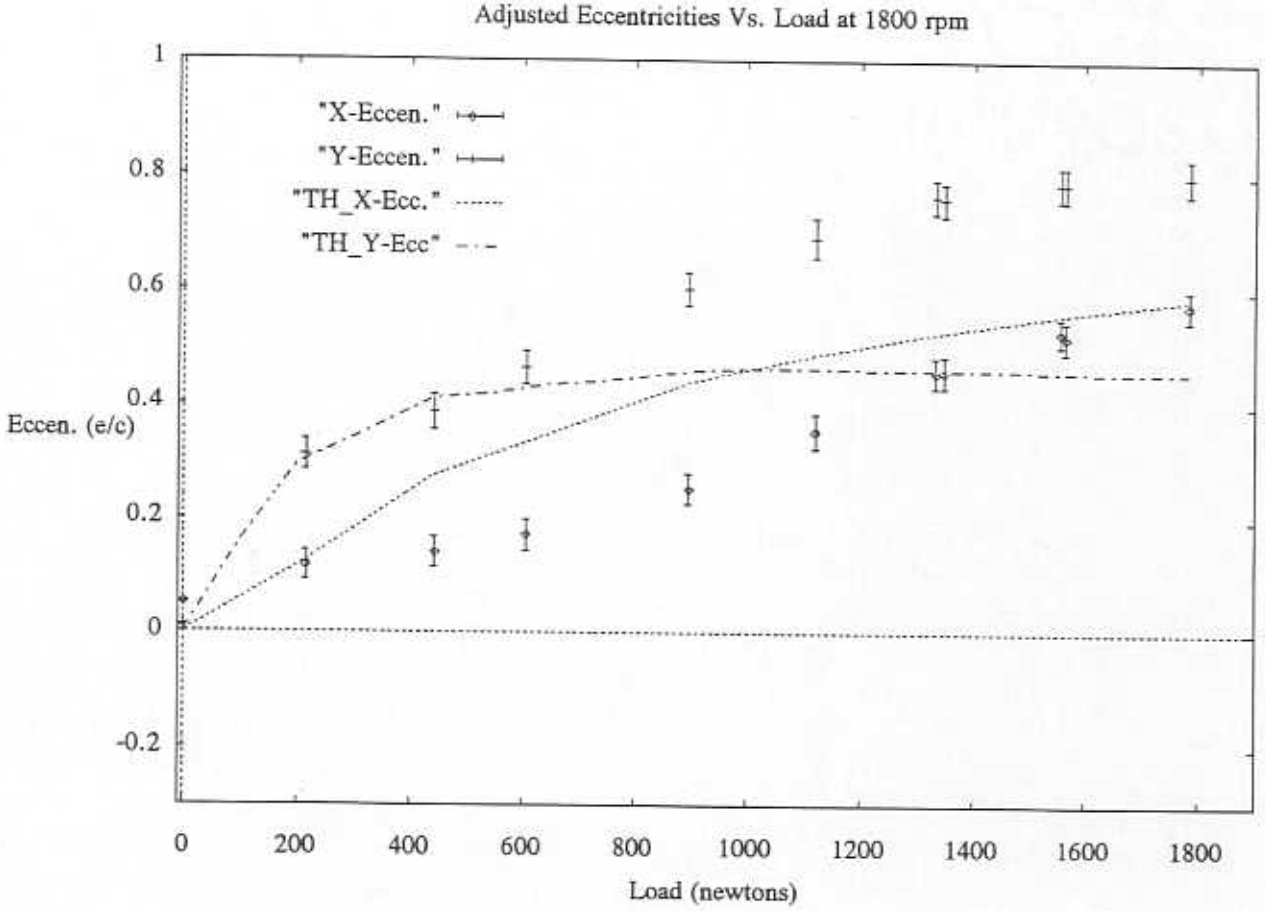

Figure 14. X and Y Direction Eccentricities for the Plain Journal Bearing Under Applied Loads at 1,800 rpm.

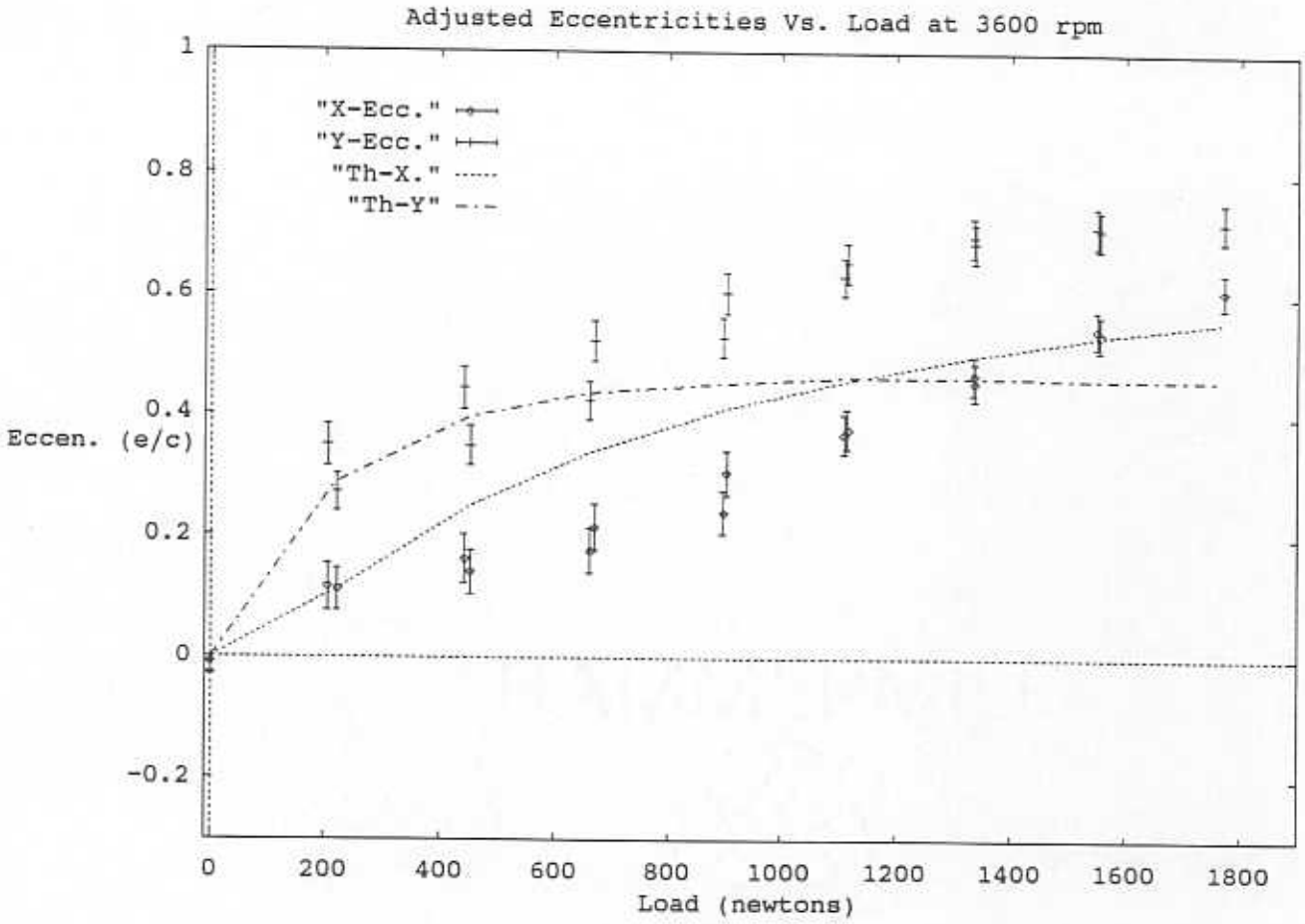

Figure 15. X and Y Direction Eccentricities for the Plain Journal Bearing Under Applied Loads at 3,600 rpm.

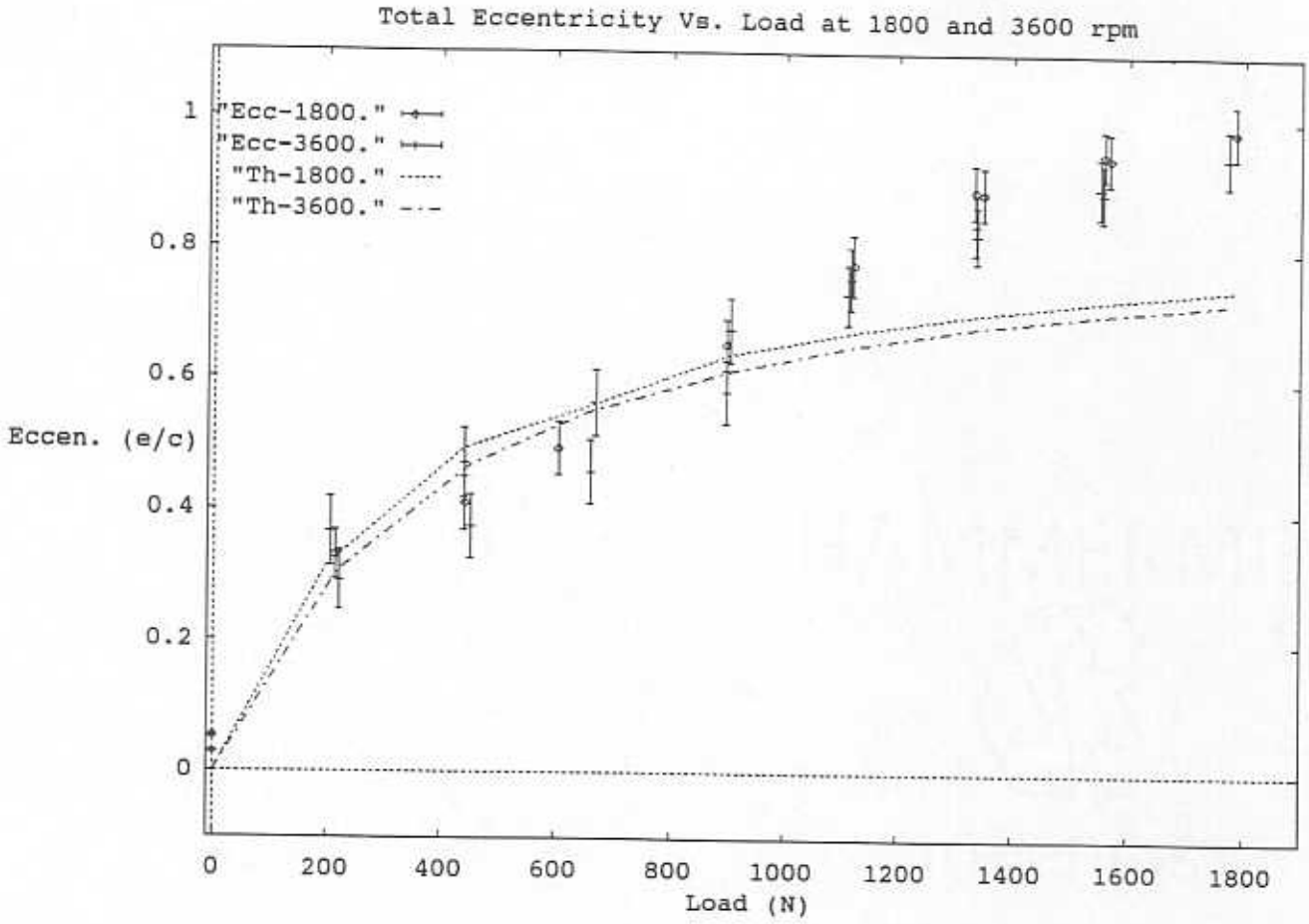

Figure 16. Total Journal Bearing Eccentricities Under Applied Loads at 1,800 and 3,600 rpm.

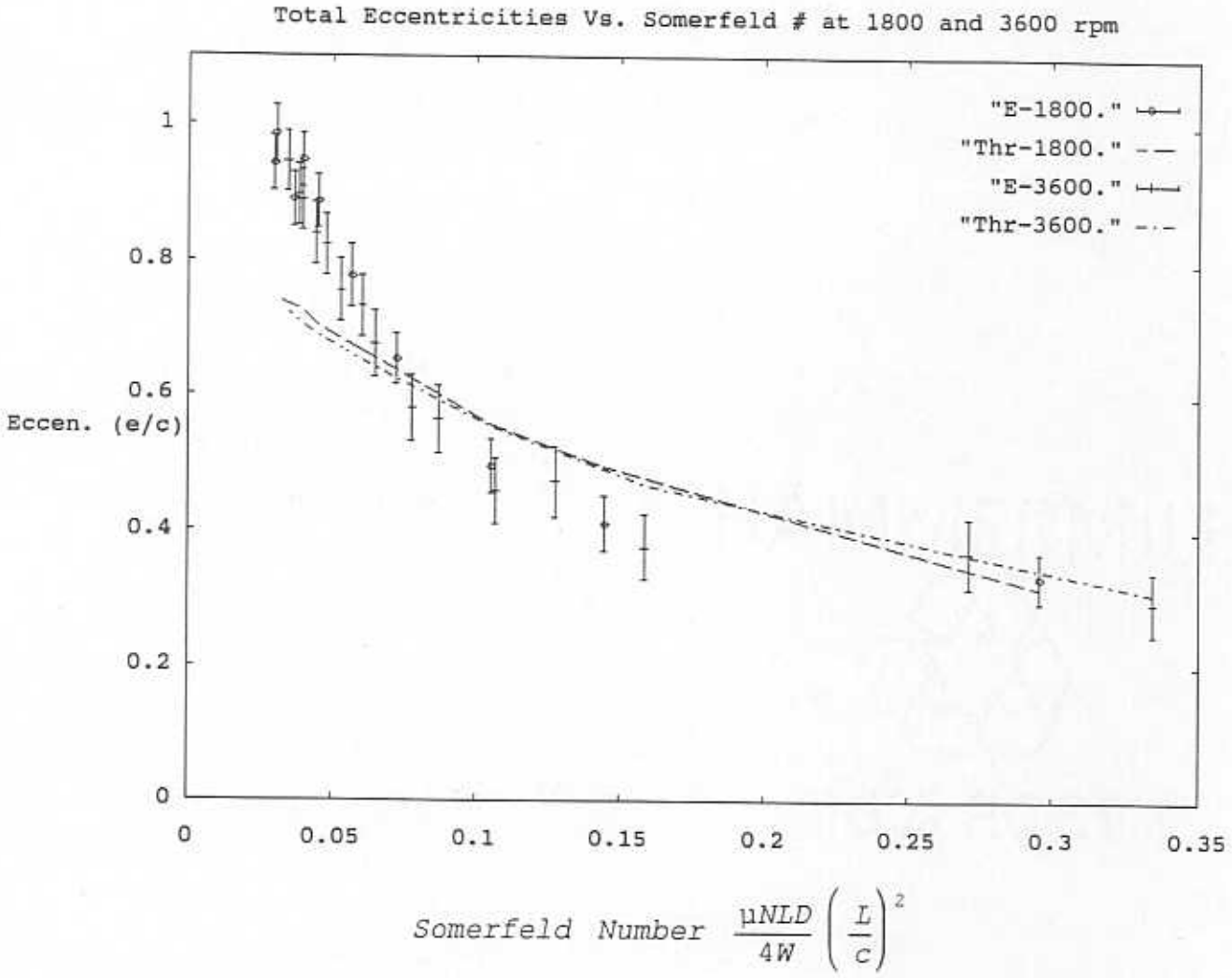

Figure 17. Total Journal Bearing Eccentricities and the Calculated Somerfeld Number at 1,800 and 3,600 rpm.

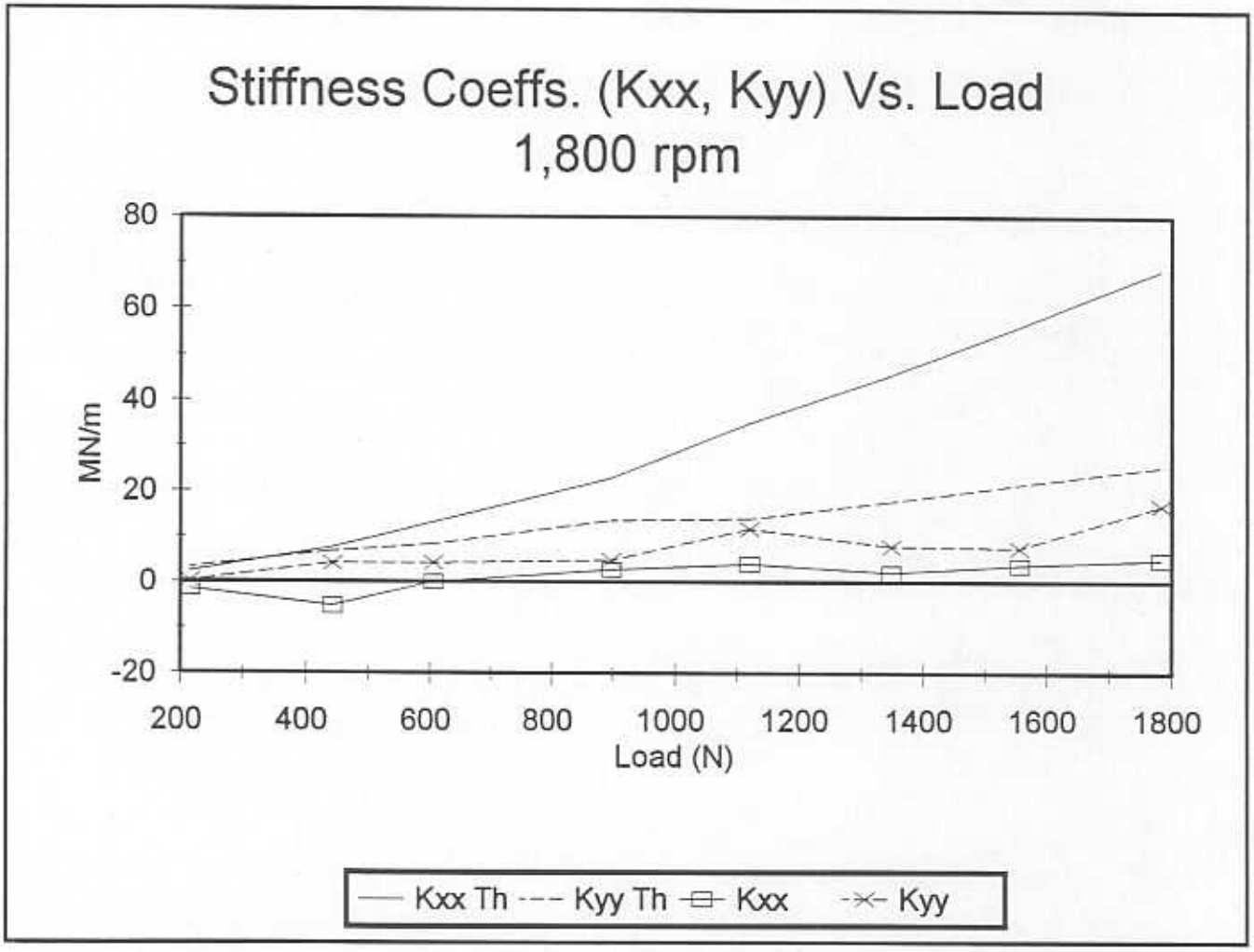

Figure 18. Direct Stiffness Coefficients (Kxx, Kyy) of the Plain Journal Bearing Under Applied Loads (Loading Only) at 1,800 rpm. Comparison of Tests and Theory.

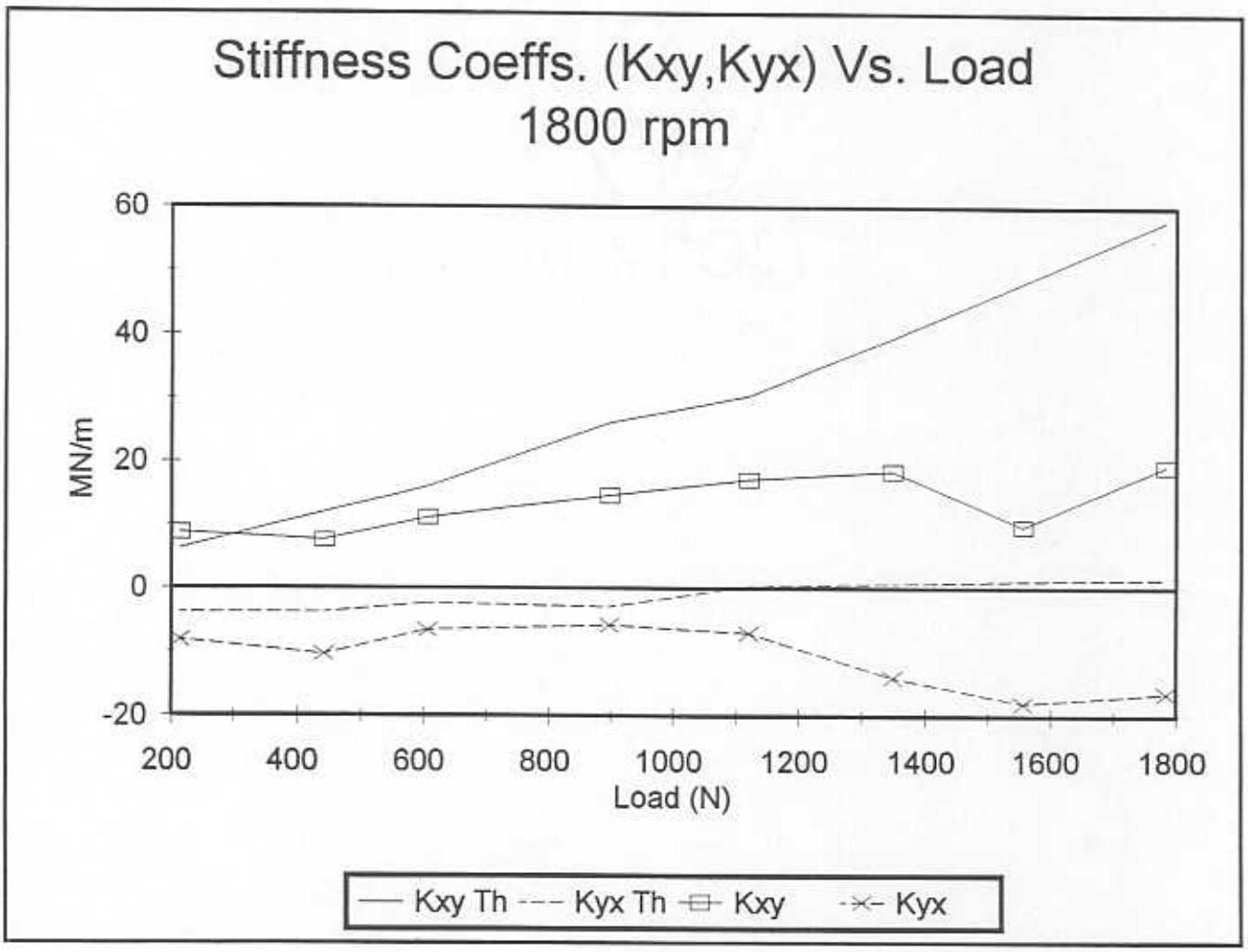

Figure 19. Cross-Coupled Stiffness Coefficients (Kxx, Kyy) of the Plain Journal Bearing Under Applied Loads (Loading Only) at 1,800 rpm. Comparison of Tests and Theory.

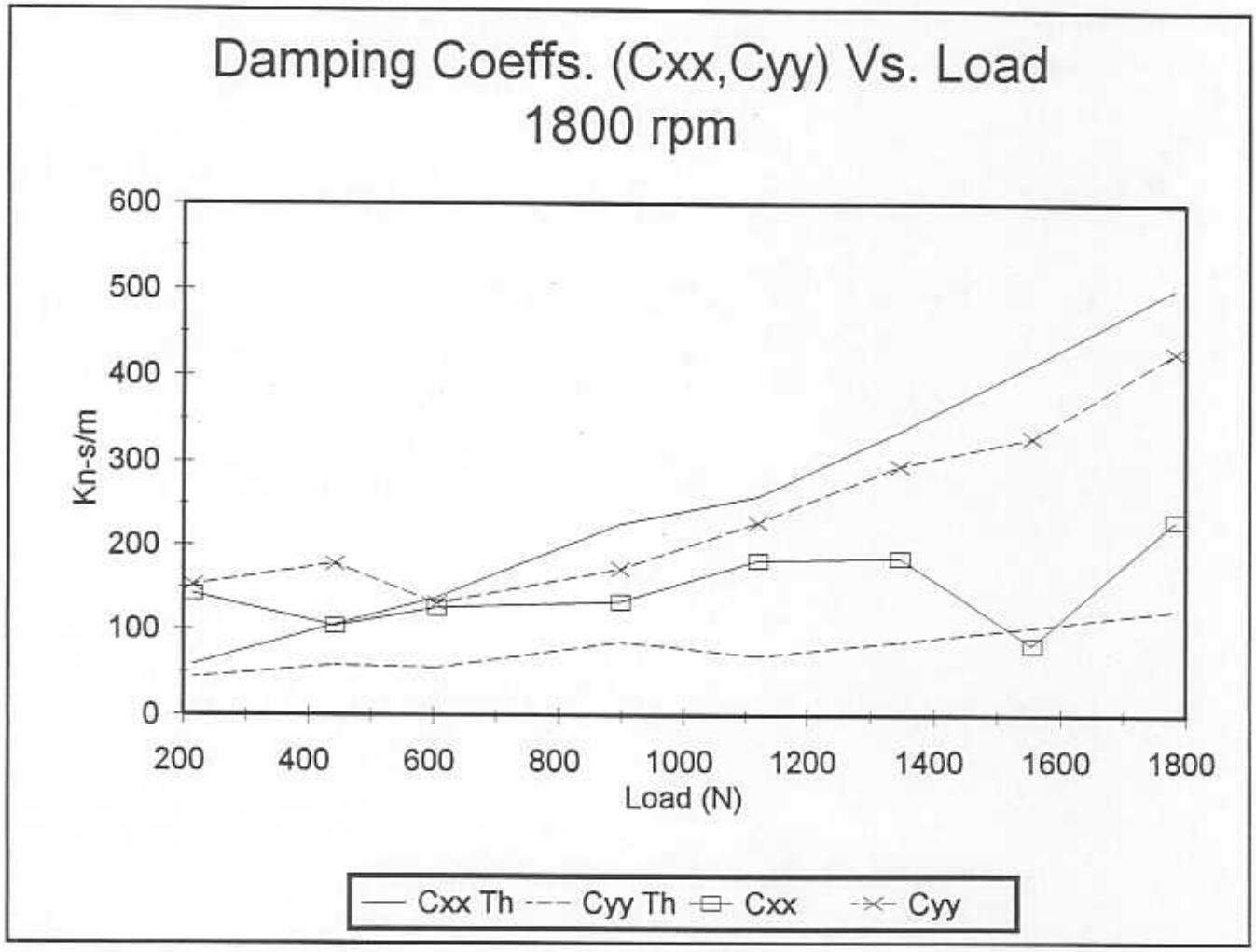

Figure 20. Direct Damping Coefficients (Cxx, Cyy) of the Plain Journal Bearing Under Applied Loads (Loading Only) at 1,800 rpm. Comparison of Tests and Theory.

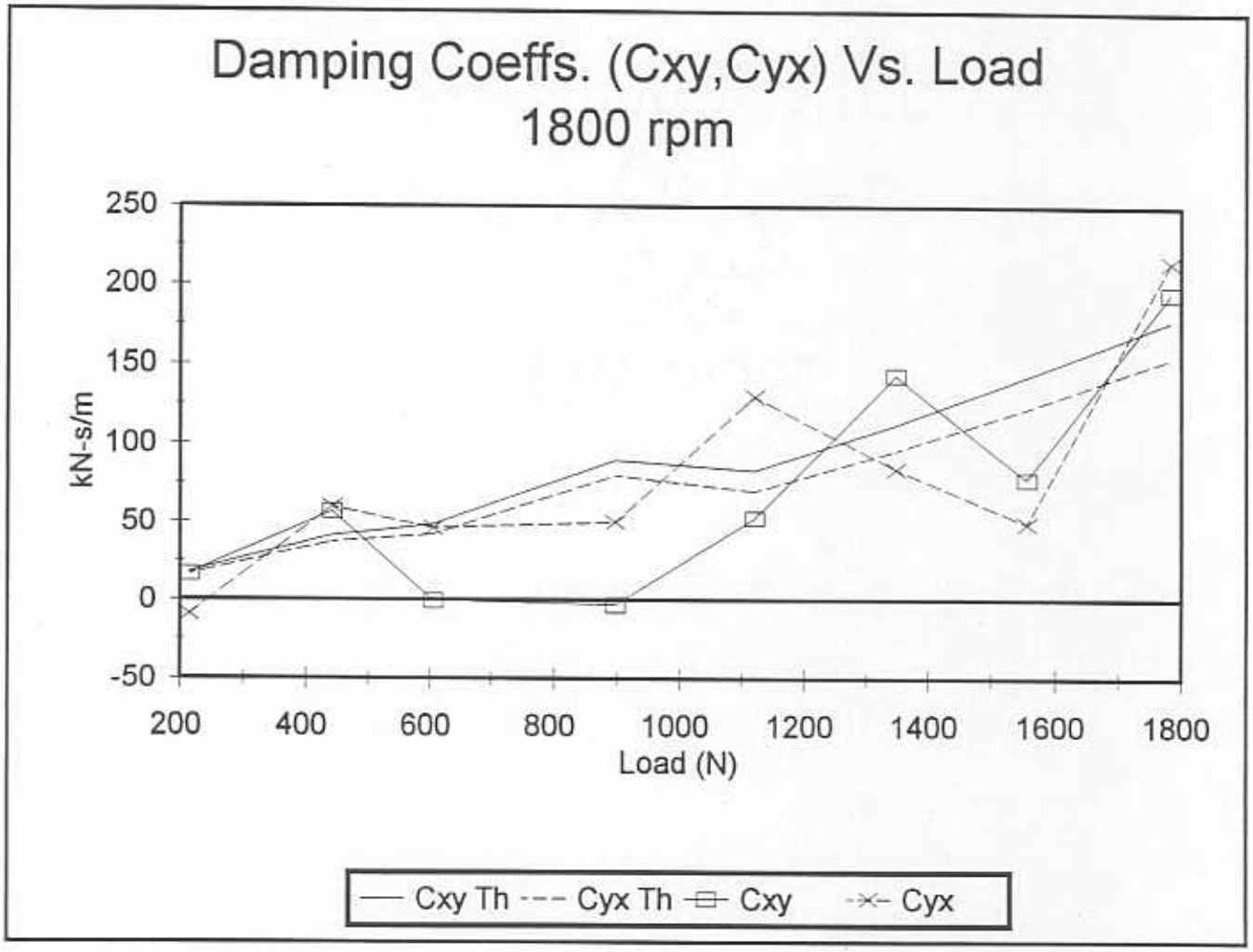

Figure 21. Cross-Coupled Damping Coefficients (Cxy, Cyx) of the Plain Journal Bearing Under Applied Loads (Loading Only) at 1,800 rpm. Comparison of Tests and Theory.

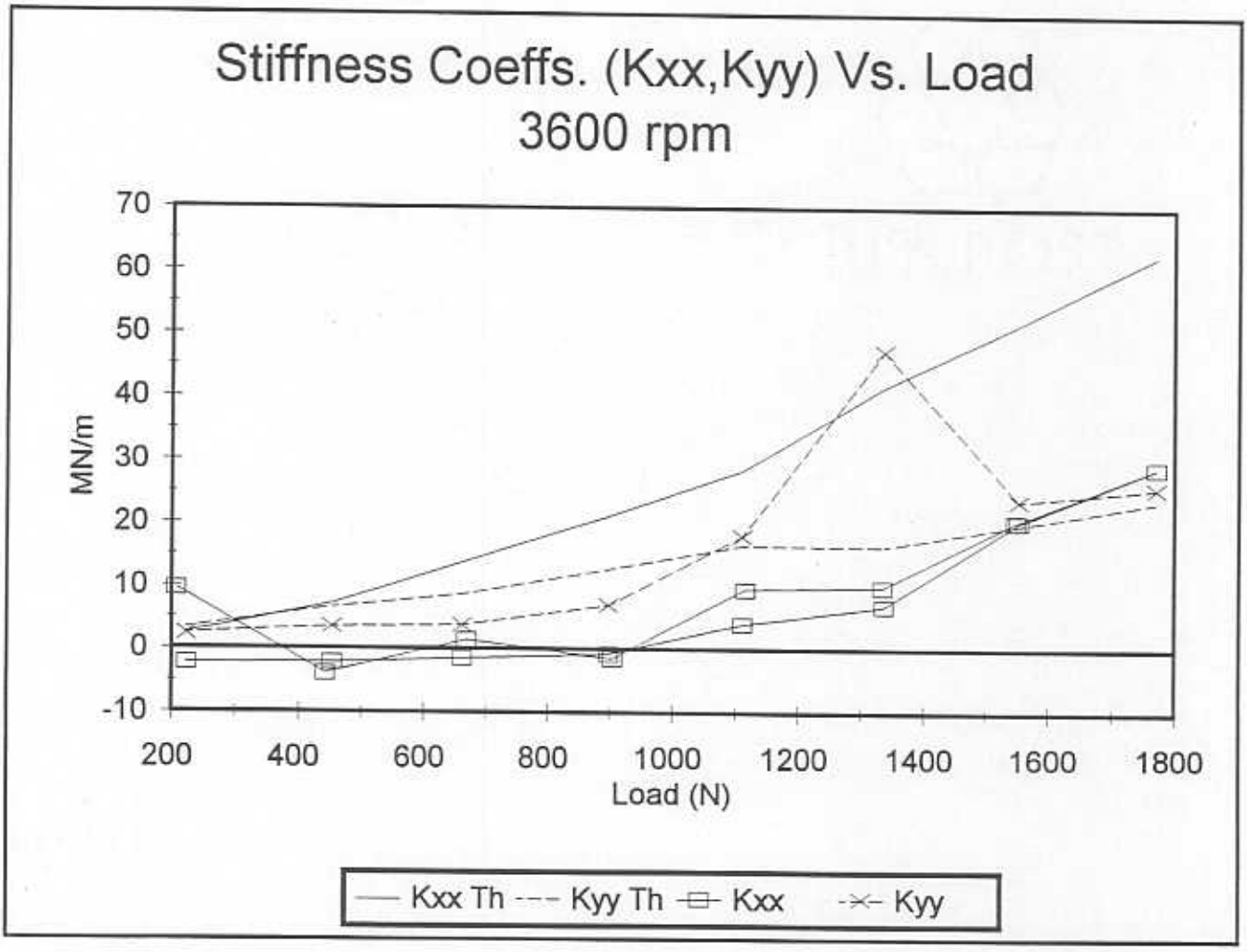

Figure 22. Direct Stiffness Coefficients (Kxx, Kyy) of the Plain Journal Bearing Under Applied Loads (Loading and Unloading Kxx Only) at 3,600 rpm. Comparison of Tests and Theory.

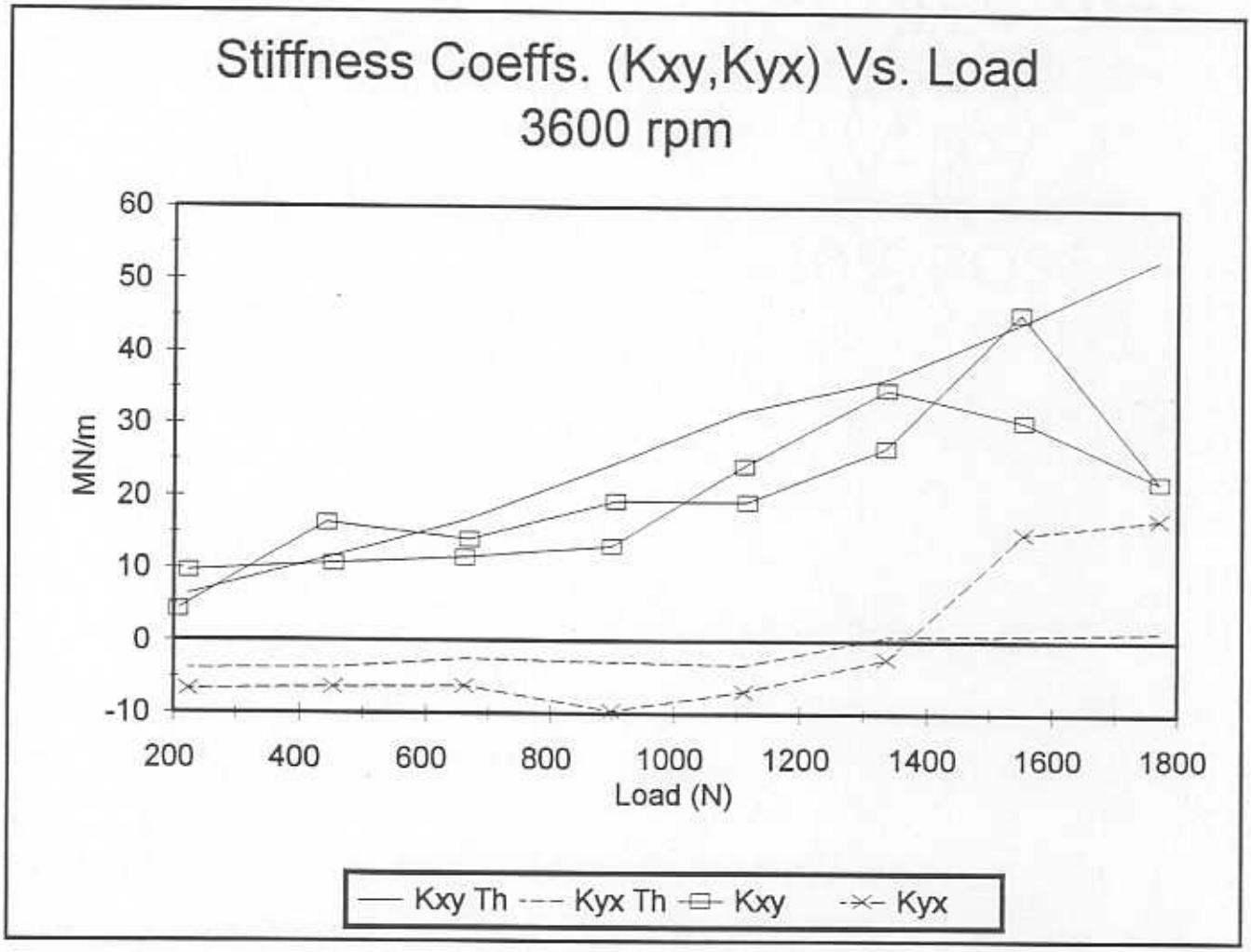

Figure 23. Cross-Coupled Stiffness Coefficients (Kxy, Kyx) of the Plain Journal Bearing Under Applied Loads (Loading and Unloading Kxy Only) at 3,600 rpm. Comparison of Tests and Theory.

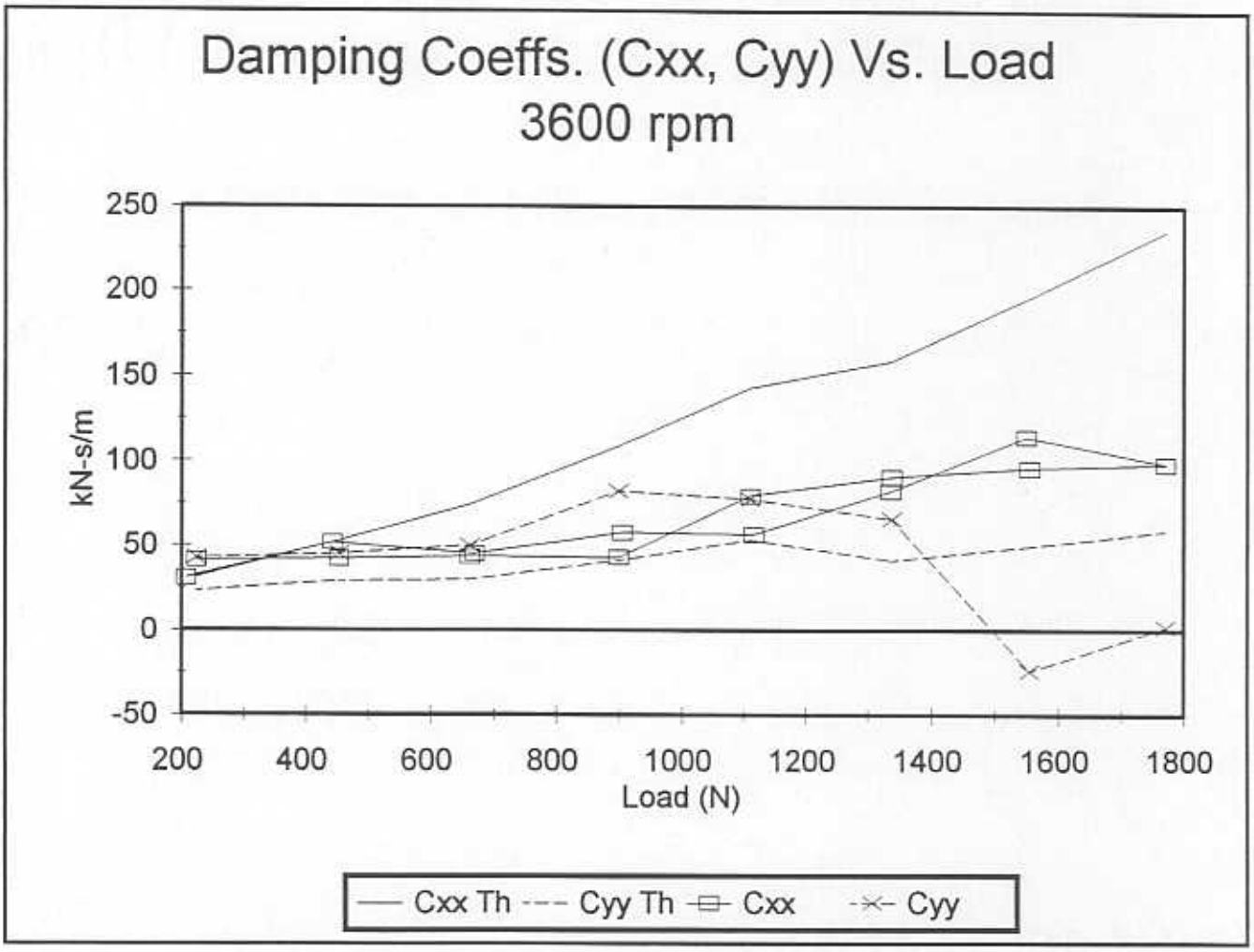

Figure 24. Direct Damping Coefficients (Cxx, Cyy) of the Plain Journal Bearing Under Applied Loads (Loading and Unloading Cxx Only) at 3,600 rpm. Comparison of Tests and Theory.

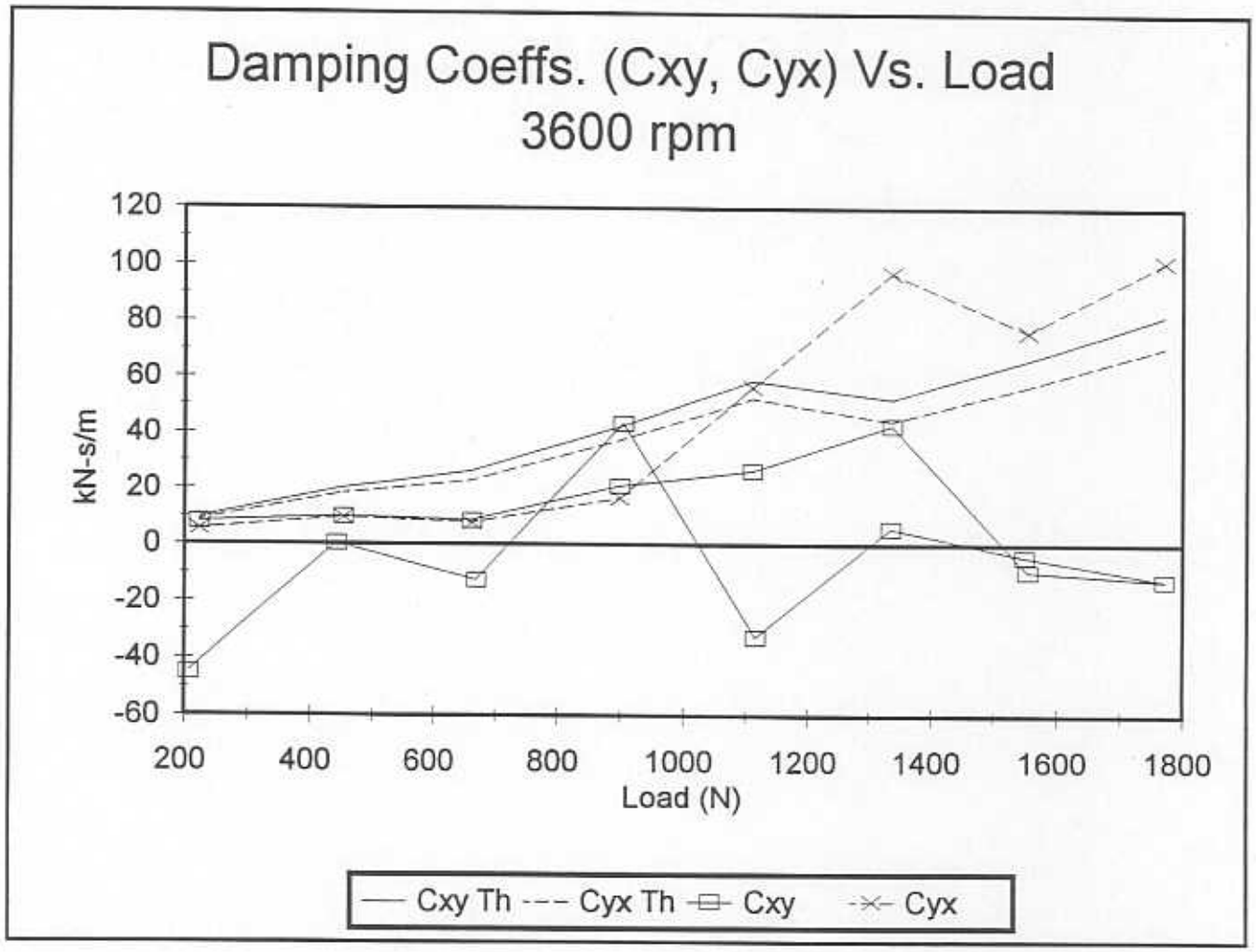

Figure 25. Cross-Coupled Damping Coefficients (Cxy, Cyx) of the Plain Journal Bearing Under Applied Loads (Loading and Unloading Cxy Only) at 3,600 rpm. Comparison of Tests and Theory.

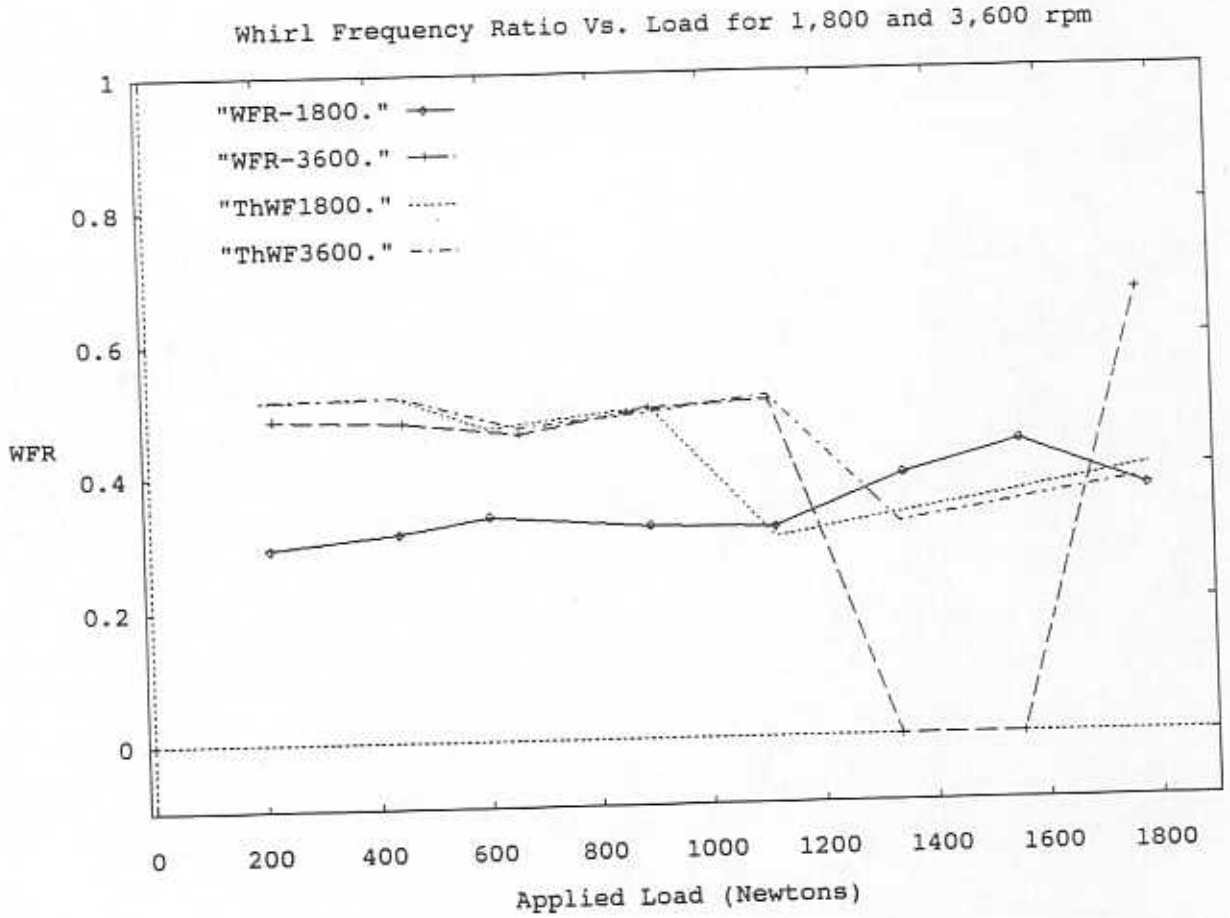

Figure 26. Plain Journal Bearing Whirl Frequency Ratio at Applied Loads for 1,800 and 3,600 rpm. Comparison of Tests and Theory.

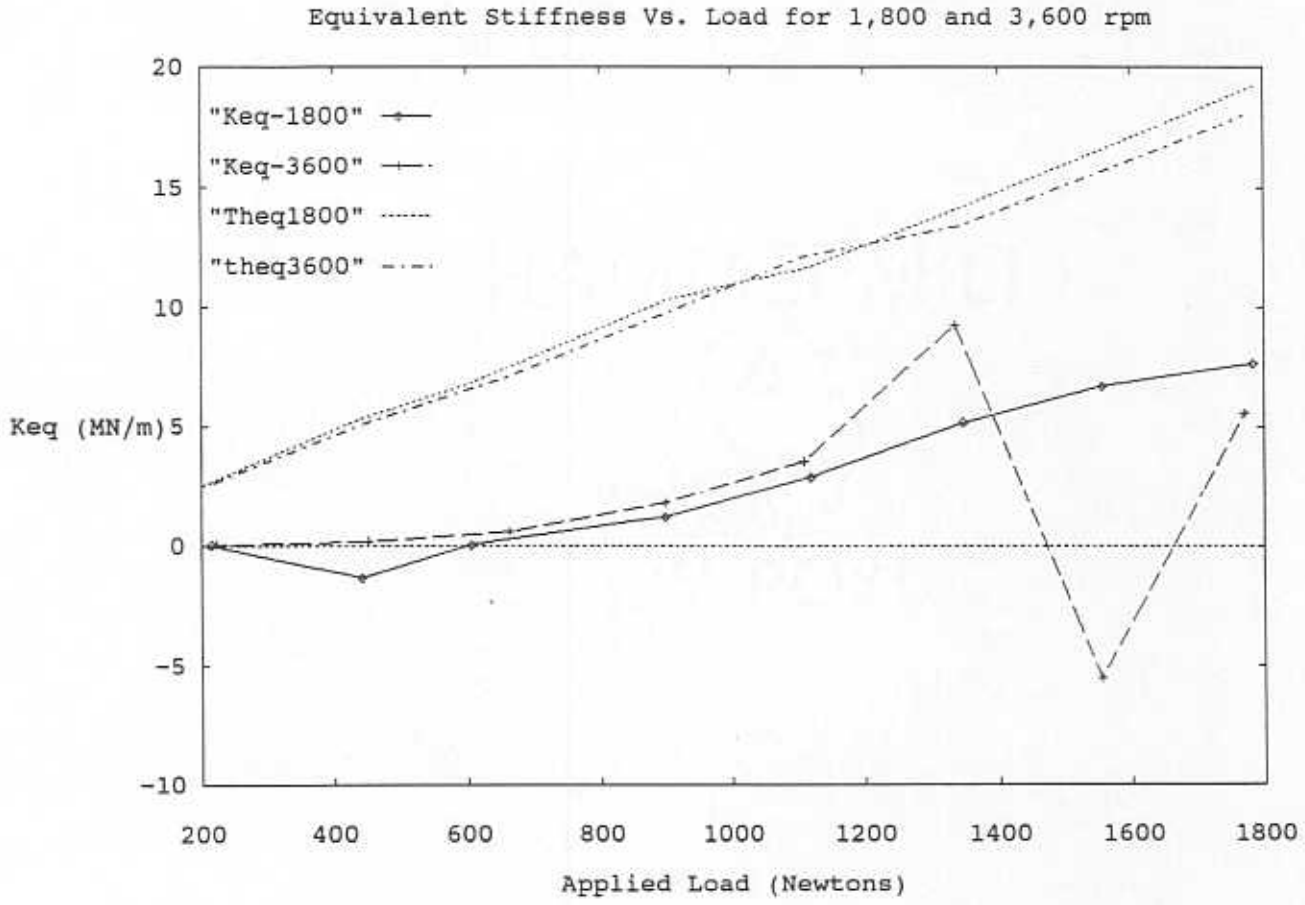

Figure 27. Equivalent Journal Bearing Stiffness at Applied Loads for 1,800 and 3,600 rpm. Comparison of Tests and Theory.

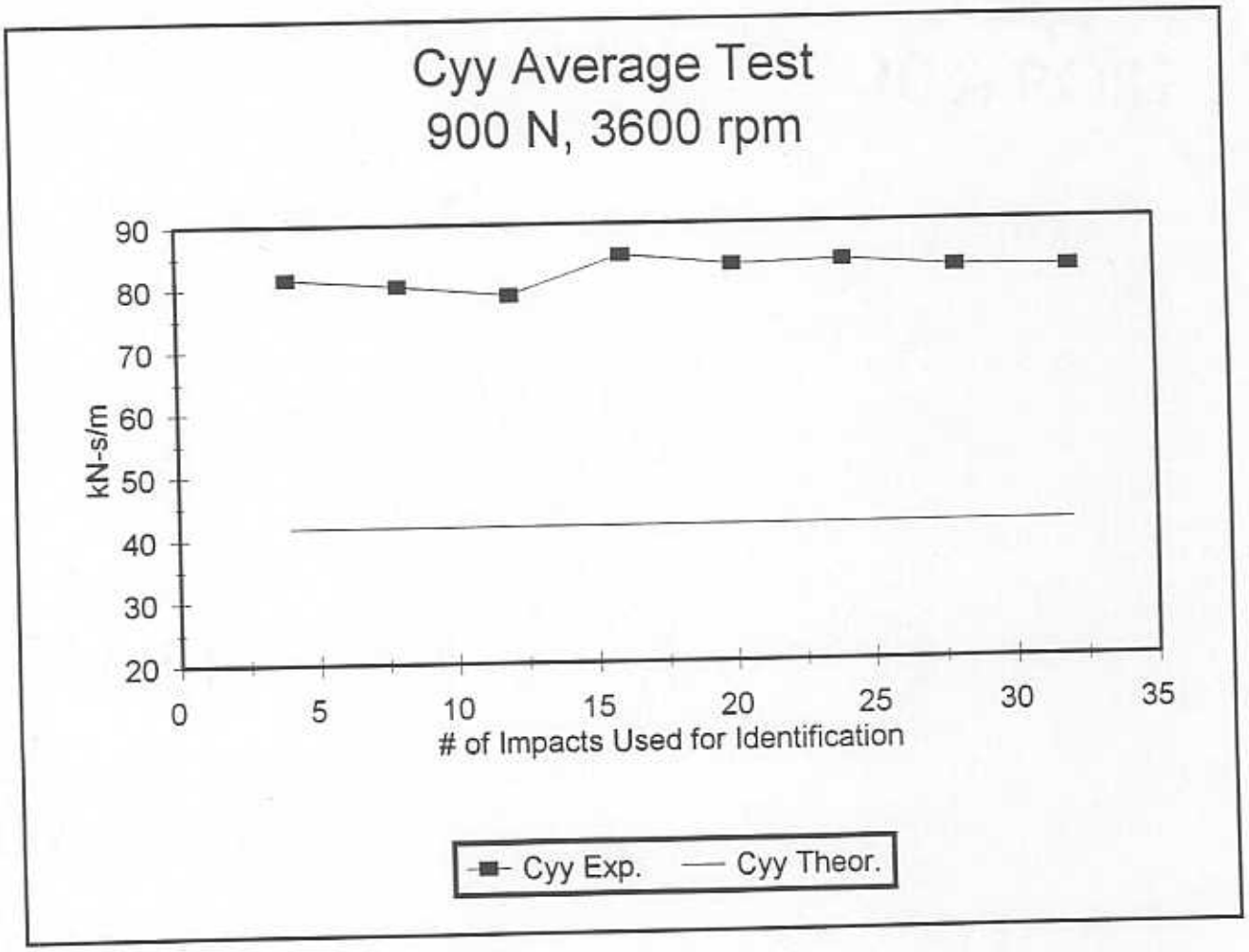

Figure 28. Typical Identified Values of Direct Damping (Cyy) in the Y Direction Using a Varying Number of Impacts. Bearing Load is 900 N at 3,600 rpm.

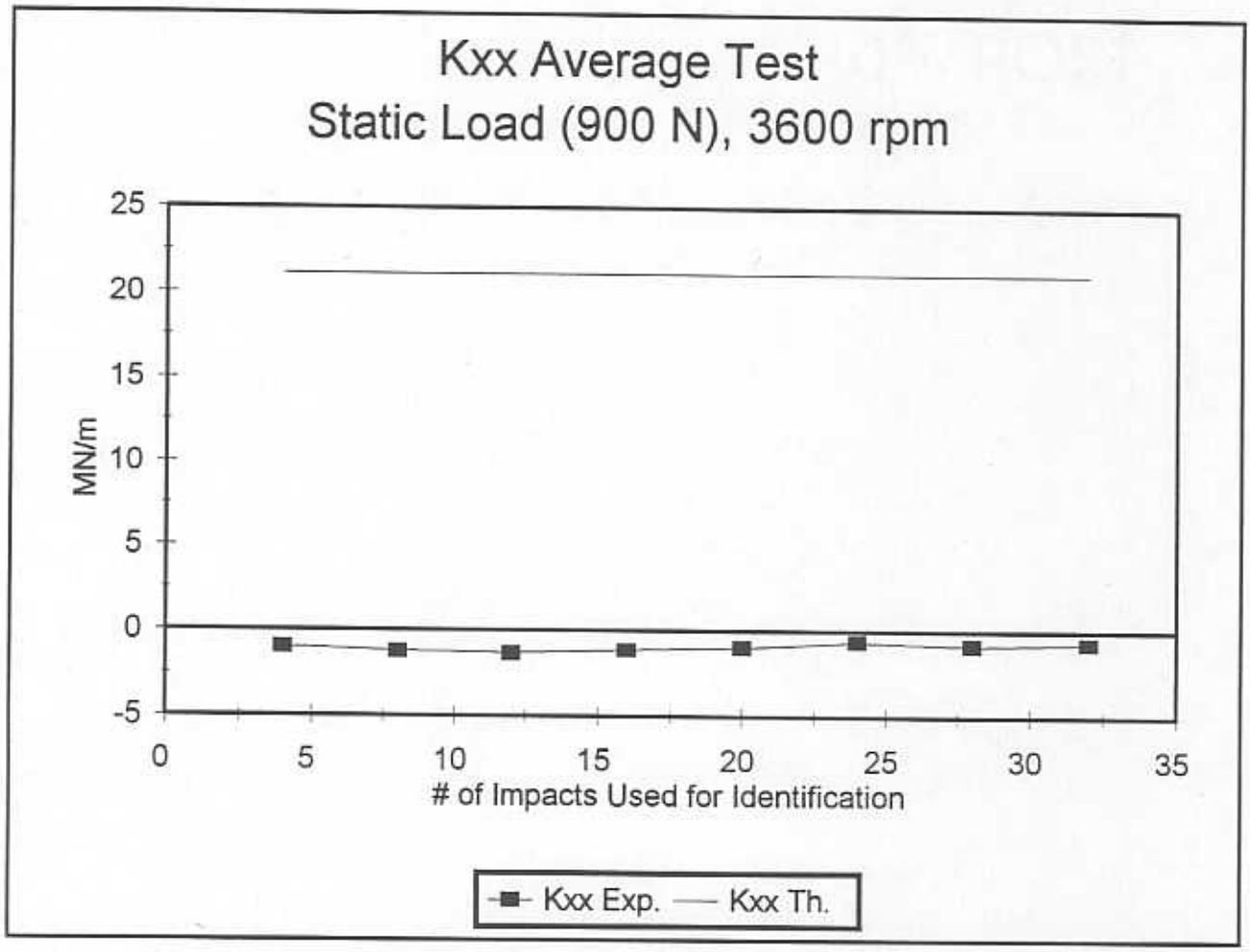

Figure 29. Typical Identified Values of Direct Stiffness (Kxx) in the Y Direction Using a Varying Number of Impacts. Bearing Load is 900 N at 3,600 rpm.

REFERENCES - PARTS I. AND II.

Childs, D., *Turbomachinery Rotordynamics, Phenomena, Modeling, & Analysis*, 1993, John Wiley & Sons, New York, pp. 132-161.

Childs, D., and K. Hale, 1993, "A Test Apparatus and Facility to Identify the Rotordynamic Coefficients of High Speed Hydrostatic Bearings," Journal of Tribology, Vol. 116,2, pp. 337-334.

Kline, S. J., and F. A. McClintock, January, 1953, "Describing Uncertainties in Single Sample Experiments," Mechanical Engineering, p. 3.

Lund, J. 1966, "Self-Excited, Stationary Whirl Orbits of a Journal in a Sleeve Bearing," Ph.D. Thesis, Rensselaer Polytechnic Institute, Troy, NY.

Nordmann, R., and K. Schöllhorn, 1980, "Identification of Stiffness and Damping Coefficients of Journal Bearings by Means of the Impact Method," IMechE Second International Conference, Vibrations in Rotating Machinery, Paper C285/80, pp. 231-258.

Pinkus, O. and Sternlicht, B., 1961, "Theory of Hydrodynamic Lubrication," McGraw-Hill, pp.12.

Ramli, M. D., J. B. Roberts, and J. Ellis, 1987, "Determination of Squeeze-Film Dynamic Coefficients from Experimental Transient Data," ASME Journal of Tribology, January, 1987, Vol. 109, pp. 155-163.

Rouvas, C., and B. T. Murphy B T, Hale R K, 1992, "Bearing Parameter Identification Using Power Spectral Density Methods," Proceedings of the Institution of Mechanical Engineers, Vibrations in Rotating, Paper C432/151, pp. 297- 303.

San Andres, L. A., "Analysis of Arbitrary Recess Geometry Hydrostatic Bearings," Proc. of the 6th NASA Conference on Advanced Earth-to-Orbit Propulsion Technology, Huntsville, Alabama, May 1994, NASA CP 3282, Vol. II, pp. 431-441.

San Andres, L. A., 1995, "Theoretical and Experimental Comparisons for Damping Coefficients of a Short Length Open-End Squeeze Film Damper," ASME Paper 95-GT-98.

San Andres, L., and J. Vance, 1986, "Force Coefficients for Open-Ended Squeeze-Film Dampers Executing Small-Amplitude Motions About an Off-Center Equilibrium Position," ASLE Transactions, Vol. 30, 1, pp. 69-76.

III. PRELIMINARY FORCE COEFFICIENTS FOR A FLEXURE-PIVOT, TILTING PAD JOURNAL BEARING

INTRODUCTION

Excessive levels of vibrations and rotordynamic instabilities can have a dramatic effect on the performance and life of turbomachines. Due to the high speeds typically encountered in the operation of these machines, the control of these problems must be a high priority or else the consequences may be catastrophic. Therefore, many of today's rotor systems utilize fluid film bearings to provide vibration control and suppress instabilities by virtue of their inherent damping characteristics.

The dynamic force characteristics of fluid film bearings can be described by twelve rotordynamic coefficients comprised of stiffness, damping, and inertia terms. These coefficients are dependent on the system operating conditions and help to distinguish how a particular type of bearing behaves when subjected to various loads, speeds, temperatures, and so on. Though these rotordynamic coefficients can be predicted theoretically for many types of hydrodynamic bearings and configurations, experimental identification always provides more realistic values and the desired verification of analytical tools.

The TRC Fluid Film Bearing Element Test Rig has been designed and constructed to facilitate testing on these types of bearings at various operating conditions. This rig enables the dynamic responses of the bearing to be recorded and then processed in the frequency domain through a parameter identification program to identify the bearing impedances for each test. Currently, the TRC Fluid Film Bearing Element Test Rig is being used to test a Flexurepivot™ tilt pad bearing

generously donated by KMC, Incorporated. Test conditions include speeds, impact loads, and static loads up to 6500 rpm, 1780 N (400 lbf), and 1335 N (300 lbf), respectively. The following report gives a brief literature review of relevant material, a detailed description of the test bearing, lists the modifications made to the test rig, presents theoretical results obtained from the hydroflext program (San Andres, 1994)for a flexure-pivot tilting-pad bearing, and summarizes the proposed work for next year.

LITERATURE REVIEW

Though there are relatively few published papers concerning flexure-pivot tilting-pad bearings, several interesting facts can be found in the archival literature. Flexure-pad bearings offer a wider range of stiffness and damping coefficients than any other type of bearing configuration (Zeidan, 1992). Zeidan also points out the complexity in design of conventional tilting-pad bearings and, in general, their lower damping characteristics versus fixed-geometry bearings. These shortcomings can be reduced by replacing them with flexure-pad bearings. Flexure-pivot tilting-pad bearings are similar in appearance to tilting pad bearings with the exception that the pads of a flexure pad bearing are structurally connected to a flexible web. This gives the flexure pads a rotational stiffness that can directly affect the stiffness coefficients of the fluid film bearing. Therefore, this parameter can be incorporated into the design to obtain a wider range of bearing coefficients.

Armentrout and Paquette (1993) examined the rotordynamic characteristics of flexure-pivot tilting-pad journal bearings and mention how flexure-pad journal bearings offer essentially the same advantages as tilting-pad bearings without being as difficult to design and manufacture. Analysis show that as the

thickness of the webs in the flexure pads increases, the stability of the flexure-pad bearing decreases and eventually approaches that of a fixed-geometry bearing. De Choudhury et al. (1992), performed tests on a high speed centrifugal compressor supported on either flexure-pad hydrodynamic bearings or tilting-pad bearings with integral taperland thrust pads. The test rig was capable of several bearing loads, various lubricant temperatures, and data was collected over operating speeds to 3750 rpm. Lower oil temperature rise, increased stability, and less frictional power loss were observed when using the flexure-pad bearing system as opposed to the tilting/thrust pad bearing configuration.

A method of calculating the dynamic force coefficients for flexure-pad journal bearings is presented by Chen (1994). This method included the flexibility of the support web and pad inertia effects. San Andres' (1994) work gives an advanced model for Flexurepivot™ tilt pad, tilting pad, and hydrostatic turbulent flow bearings for cryogenic environments and applications.

Several important facts can be inferred about flexure-pivot tilting-pad bearings from literature concerning conventional tilting-pad bearings due to their similarities during operation. Several investigations have been conducted in the past aimed at identifying the rotordynamic coefficients for tilting-pad bearings. Parkins and Horner (1992) experimentally measured the stiffness coefficients for a five shoe, central-pivoted tilting-pad bearing for rotational speeds of 3000 - 8000 rpm and static loads varying from 0.5 - 5.0 kN. The presence of significant cross-coupled terms under certain operating conditions was an interesting result from this investigation.

Arumugam et al (1994) experimentally identified the stiffness and damping coefficients for two, four-pad tilting-pad

bearings with different configurations and one 360 degree cylindrical journal bearing. Here the rotor was excited using an unidirectional sine sweep perturbation force method over a range of shaft rotational speeds. Loads were applied in the two principal loading configurations of load on and load between pads and it was found that the test bearings demonstrated anisotropic behavior for the two loading directions. The correlation between experimentally determined rotordynamic coefficients and theoretical values was reasonable and the inertia force coefficients of the oil film were found to be negligible.

Parsell et al (1982) theoretically examine the effects of damped vibrational frequencies on the linear reduced rotordynamic coefficients for a five shoe, tilting-pad journal bearing. The authors concluded that synchronously reduced bearing coefficients are reasonably accurate for the calculations of damped eigenvalues except for zero preloads and large Sommerfeld numbers. It was also deduced that a complete set of dynamic coefficients should be used when modeling a tilting pad bearing with zero preload.

Nicholas et al (1977) present theoretical stiffness and damping coefficients using finite elements and the pad assembly method for a five pad tilt-pad bearing subjected to various operating conditions. Important conclusions were the fact that the top-unloaded pad for this chosen bearing configuration does in fact contribute to the damping characteristics in all cases and to the stiffness only when the pads are not centrally pivoted. Increasing bearing preloads increase the bearing stiffness and eliminate structural asymmetry at high Sommerfeld numbers.

TEST BEARING DESCRIPTION

As previously mentioned, the TRC Fluid Film Bearing Element

Test Rig is currently being utilized to test a Flexurepivot™ tilt pad bearing donated by KMC, Incorporated. A schematic view of this bearing is shown in **Figure 30**. The clearance between the backside of each pad and the rest of the bearing has been exaggerated for clarity. The actual clearance is about 0.3048 mm (0.012 in). The inner diameter of the bearing measured between the pads at the web points is on average 127.188 mm (5.0074 in) and each pad has an arc length of 80° with a 10° space between each pad. **Table 2** gives a complete list of measurements along with other parameters such as the bearing L/D ratio, journal diameter, and weights of various components of the test rig. The dimensions listed on **Figure 30** are the actual values measured before installation of the bearing into the TRC Test Rig. **Figure 31** shows the coordinate system, load direction, pad designation, thermocouple locations, and a cross sectional view of the bearing as seen from above the test rig. The journal rotation is counter-clockwise (ccw) with respect to this figure and the clearance between the journal (not shown) and the pads is on average 0.1384 mm(0.00545 in).

The thermocouples (T1 - T8), see **Figure 31**, are mounted on the leading and trailing edge of each pad on the axial centerline since this is the location of the maximum temperature and pressure for tilting-pad bearings (Nicholas, 1994). The oil inlet and discharge temperatures are also measured which, when coupled with the flow rate measurements, give the frictional power loss of the bearing for a particular experiment. This procedure is very similar to the method used by De Choudhury and Masters (1983).

Not included in these figures are two sets of three counter bores located on the outer portion of the bearing along the axial centerline. These counter bores enable the Flexurepivot™ tilt pad bearing to be supported in such a way that both load on pad

(LOP) and load between pads (LBP) configurations can be tested on the TRC Test Rig. The LBP configuration is currently in place, as seen in **Figure 31.**

The design and manufacturing of flexure-pivot tilting-pad bearings are two of the main differences between these bearings and conventional tilting pad bearings. Typically, flexure pad bearings are constructed out of a solid blank via an electric discharge machining process, which gives the bearing a one piece design (De Choudhury et al, 1992). This feature gives flexure pad bearings a distinct advantage over conventional tilting pads since the numerous parts involved in the manufacturing of such bearings are eliminated. The test Flexurepivot™ tilt pad bearing is fabricated out of low carbon steel and designed with a rotational (web) stiffness of 1129.08 N m/rad for each pad. This rotational stiffness provides a minimal difference in the cross coupled stiffness coefficients (Kxy-Kyx). Note that the destabilizing energy introduced into the system is a product of the whirl orbit area and the net value of (Kxy-Kyx) (Zeidan, 1992).

TRC TEST RIG MODIFICATIONS

The first part of this report contains a complete description of the TRC Fluid Film Bearing Element Test Rig used for the experimental identification of the rotordynamic coefficients of various hydrodynamic bearings. Since this test rig was designed to be compatible with various fluid film bearings, very few modifications were necessary to make it suitable for the Flexurepivot™ tilt pad bearing. The only changes required in the test rig itself consisted of the machining and installation of a new bearing housing base plate and bearing housing cap. The shoulder on the original bearing housing base plate supporting the test bearing would have

hindered the deflections of the pads on the new bearing. Therefore, a base plate was constructed with the appropriate outer diameter and a shoulder that protruded to the beginning of the webs on the bearing. A new bearing housing cap was also designed and manufactured to allow for additional oil inlet lines to increase the amount of oil fed into the bearing housing. This new cap allows for either one large oil inlet line at the center, three smaller lines equally spaced around the outer edge of the cap, or both.

One other modification to the test rig was the polishing of the top part of the rigid vertical shaft to reduce the amount of runout (noise) present in the signals taken by the proximity probes. This runout is most likely due to minute scratches on the surface of the shaft itself. The procedure allowed the runout of the shaft to be reduced from 0.033 mm (0.0013 in) to 0.019 mm (0.00075 in).

Finally, modifications had to be made on the test bearing itself after preliminary tests demonstrated that there was clearly not a complete oil film present between the journal and each pad. This conclusion was reached by running the rig up to a speed of 4,000 rpm with oil flowing into the bearing housing, statically loading the bearing, and observing its response. The bearing could only withstand static loads in the neighborhood of 445 N (100 lbf) before the journal would approach the maximum radial clearance of the bearing. Once the bearing had been removed, it was apparent that a considerable amount of rubbing on pad # 3 had taken place. The loss of material was approximately 0.0127 mm (0.0005 in) on both the surface of this particular pad and on the journal.

Other peculiar occurrences noticed were the location of the equilibrium position of the journal within the bearing, and a random low frequency rotational movement of the bearing housing

when the shaft was running at a constant speed with no static load present. The equilibrium position was shifted almost completely over to one side of the bearing for the most part, but would randomly jump or whirl at a very low frequency throughout the tests. This random motion tended to correspond to a jerking rotational movement in the bearing housing in which the housing would rotate in the direction of the journal rotation and then oscillate back to its original position. This unusual displacement would continue for about 5-10 seconds before eventually coming back to rest. It was concluded that the manner in which the oil inlet line was attached to the bearing housing cap, along with the high oil flow rate, were generating a moment on the bearing housing leading to the re-occurring rotational oscillations. This problem was remedied by attaching the oil feed line at the center of the bearing housing cap and reducing the flow rate so that this moment could not be generated.

Originally it was thought that the viscous shearing forces between the oil and the rotating journal would be enough to pull oil into the film and create a uniform fluid film. The bizarre movement of the journal equilibrium position and the unexpected low stiffness values of the bearing were caused by the lack of a complete oil film in the bearing pad journal interfaces. This problem appears to have been corrected by attaching end plates on the bottom side of the bearing in such a way that the axial flow of oil could be reduced. A cross sectional side view of the test bearing assembly with an end plate installed to reduce the axial flow is shown in **Figure 32**. Also seen in this figure are the direction of oil flow into the bearing housing, the location of the fluid film, and the troublesome channels between the trailing and leading edges of the pads. A great deal of care was taken during the installation of the end plates to insure that the clearance between the plates and the bottom of the bearing were

small (0.0762 - 0.127 mm; 0.003 -.005 in) but still did not interfere with the deflections of the pads. The addition of these plates now allows a pool of oil to be present between all the pads at all times. These pools will provide an oil source that can be easily pulled into the film by viscous shearing. Also, four additional radial holes were drilled in the bearing to aid in the injection of oil into the bearing. These holes are 4.17 mm (0.1640 in) in diameter and are located on the axial centerline between each pad (see **Figures 30 and 31**).

THEORETICAL RESULTS

Theoretical results for a flexure-pivot tilting-pad bearing are obtained by using the hydroflext program (San Andres, 1994). This computational tool provides numerical predictions for the dynamic force coefficients for a selected bearing configuration and operating conditions. Solutions for pressure, flow, temperature, film forces, among others are also determined.

The dynamic force coefficients of the test bearing are of particular interest since these are the parameters to be identified experimentally. However, a vast amount of other information enables the user to gain a great deal of insight into the behavior of a flexure pad bearing under certain operating conditions. **Table 3** shows bearing geometry parameters and operating conditions used for the Flexurepivot™ tilt pad bearing case. Once an input file containing this information is created, the user has several options as to what to do next. Typically, the solution for the centered position and no misalignment is obtained first in order to have an approximate guess for the future iteration process necessary to solve cases with specified values of eccentricity. **Table 4** lists typical results from the program for a shaft speed of 4000 rpm and two different static loads. The information listed on this table can be used to

generate curves such as those seen in **Figures 33 - 36.** These figures give an excellent overview of the theoretical behavior of this particular type of fluid film bearing when subjected to an increasing static load between pads #2 and #3. **Figure 33** shows the pad rotations for increasing static loads. Pad # 3 absorbs most of the static load in all cases, while pad # 4 remains completely motionless.

Figure 34 gives the operating journal eccentricities (e_x and e_y) of the bearing. The results show how the journal exhibits very little displacement in the direction (Y) orthogonal to the applied load, which is an indication of negligible cross-coupling effects in the bearing. **Figure 35** illustrates how the synchronously reduced cross coupled stiffness coefficients are practically nil for all applied static loads. Since these particular stiffness coefficients are directly related to the amount of destabilizing energy present in a bearing (Zeidan, 1992), it can be concluded that the Flexurepivot™ tilt pad bearing will be stable for static loads (LBP) up to 10,000 N while operating at 4,000 RPM.

The synchronously reduced damping coefficients are found in **Figure 36.** This figure depicts a linear relationship between the damping coefficients and the applied static loads. Again, as in **Figure 35,** the cross-coupled terms are relatively negligible for static loads up to 10,000 N.

A single degree of freedom (SDOF) analysis using the actual bearing assembly mass (9.70 kg) and predicted stiffness and damping values from the hydroflext program was performed. It appears that for this bearing-mass configuration, the system will be consistently overdamped since the values of the direct damping coefficients are at least 2.8 times greater than the critical damping of the simple system. It may be inferred from this fact that an oil with lower values of viscosity must be used in order

to obtain system dynamic responses with high signal to noise ratios.

The numerical predictions from the hydroflext code will serve to give an estimation of expected values when actually testing the Flexurepivot™ tilt pad bearing under similar conditions. For example, a ballpark figure of the maximum static load the bearing can handle at a certain running speed will be known, allowing limits to be set above which the bearing cannot operate safely. Moreover, this computational program gives some form of comparison for many of the parameters that will be measured and/or identified during testing of the bearing.

PROPOSED WORK

The next logical step in this investigation is to complete the trouble-shooting process regarding the preparation of the TRC Fluid Film Bearing Element Test Rig and conduct the static and dynamic tests on the Flexurepivot™ tilt pad bearing for a load between pads case. Shaft speeds will be in the range of 1,800 - 6,000 rpm using Velocite # 10 ISO VG 22 oil. Once satisfactory data have been collected, the rotordynamic coefficients identified for each case will be compared to those obtained from the hydroflext program. Future experiments will then be conducted for **load on pad** configurations, which may include a different oil and/or the use of shakers to provide the necessary dynamic loads.. This different method of dynamic loading is recommended for future tests since it will allow for system responses of enough magnitude and duration to extract accurate force coefficients.

CONCLUSIONS

There are many powerful analytical and computational programs in today's engineering society that are very useful and

versatile. These tools certainly enhance the understanding of how particular systems and/or components will behave theoretically under certain operating conditions or environments. However, without the continued practice of experimental work to support and verify these tools, engineers can never be fully confident about how a system actually performs. Furthermore, several important observations can be drawn from experimental work that could never be realized with theoretical analysis. In short, neither one of these methods can ever reach its full potential without the other.

Continued funding for this project will provide the resources necessary to advance both the experimental and theoretical phases of research for the Flexurepivot™ tilt pad bearing and others. The information collected from this investigation will definitely provide valuable knowledge and insight into the dynamic characteristics of flexure pad bearings.

Table 2: Flexure Pivot Tilt Pad Bearing and Journal Measurements

Average Inner Diameter Between Pads 1&3	127.18 mm	(5.0070 in)
Average Inner Diameter Between Pads 2&4	127.20 mm	(5.0078 in)
Overall Average Inner Diameter	127.19 mm	(5.0074 in)
Overall Bearing Length	45.87 mm	(1.8060 in)
Length-to Diameter Ratio (L\D)	0.3607	
Average Journal Outer Diameter	126.911 mm	(4.9965 in)
Average Radial Clearance	0.13843 mm	(0.00545 in)
Bearing Mass	4.117 kg	(9.076 lb)
Bearing Housing Mass	1.867 kg	(4.116 lb)
Bearing Housing Cap Mass	2.877 kg	(6.342 lb)
Mass of Oil in Bearing Housing	0.839 kg	(1.850 lb)
Total Mass	9.70 kg	(21.384 lb)

Table 3: Flexure Pivot Tilt Pad Bearing

Theoretical Operating Conditions

Bearing Geometry	
Diameter	127.188 mm (5.0074 in)
Effective Axial Length	45.72 mm (1.8000 in)
Number of Pads	4
Pad Leading Edge locations	5, 95, 185, 275 degrees
Pad Trailing Edge locations	85, 175, 265, 355 degrees
Pad Arc Lengths	80 degrees
Pad Rotational Stiffness	1129.08 N m/rad
Direction of Static Load	Load Between Pads (LBP)
Pad Offset	0.5
Preload	0.1 e-05 m
Radial clearance	138 μm
Operating Conditions	
Shaft speed	4000 RPM
Oil Inlet Pressure	0.1034 MPa
Oil Discharge Pressure	0.1034 MPa
Operating Fluid	Velocite # 10 ISO 22 Oil
Fluid Average Temperature	303.0 Kelvin (30 degrees C)
Effective Oil Viscosity	0.018 Pa s
Temperature-Viscosity Coefficient of Oil	0.0303 (1/Kelvin)
Oil Density	856 kg/m^3

Table 4: Typical Output From hydroflext Program

Shaft Speed: 4000 RPM (66.7 Hz)

Static Load = 200 N	Static Load = 1000 N
X eccentricity: 0.08759	X eccentricity: 0.42248
Y eccentricity: 0.03001	Y eccentricity: 0.03579
Total eccentricity: 0.09259	Total eccentricity: 0.42399
Pad # 1 Rotation:-0.1085e-03	Pad # 1 Rotation: -0.5335e-03
Pad # 2 Rotation: 0.6237e-04	Pad # 2 Rotation: -0.1104e-03
Pad # 3 Rotation: 0.3294e-03	Pad # 3 Rotation: 0.1140e-02
Pad # 4 Rotation: 0.7503e-24	Pad # 4 Rotation: 0.7503e-24
Fluid Reaction Force: 199.57 N	Fluid Reaction Force: 999.65 N
Fluid Reaction Force Angle: 0.150 degrees	Fluid Reaction Force Angle: 0.002 degrees
Synchronously Reduced Coefficients	
Kxx = 2.292 (MN/m)	Kxx = 13.75 (MN/m)
Kyx = -0.8723 (MN/m)	Kyx = 0.2498 (MN/m)
Kyy = 3.001 (MN/m)	Kyy = 14.69 (MN/m)
Kxy = 1.213 (MN/m)	Kxy = 2.776 (MN/m)
Cxx = 33.07 (kN s/m)	Cxx = 44.64 (kN s/m)
Cyx = 6.567 (kN s/m)	Cyx = 8.082 (kN s/m)
Cyy = 34.01 (kN s/m)	Cyy = 45.38 (kN s/m)
Cxy = -0.8590 (kN s/m)	Cxy = 2.235 (kN s/m)
Whirl Frequency Ratio: 0.069	Whirl Frequency Ratio: 0.048

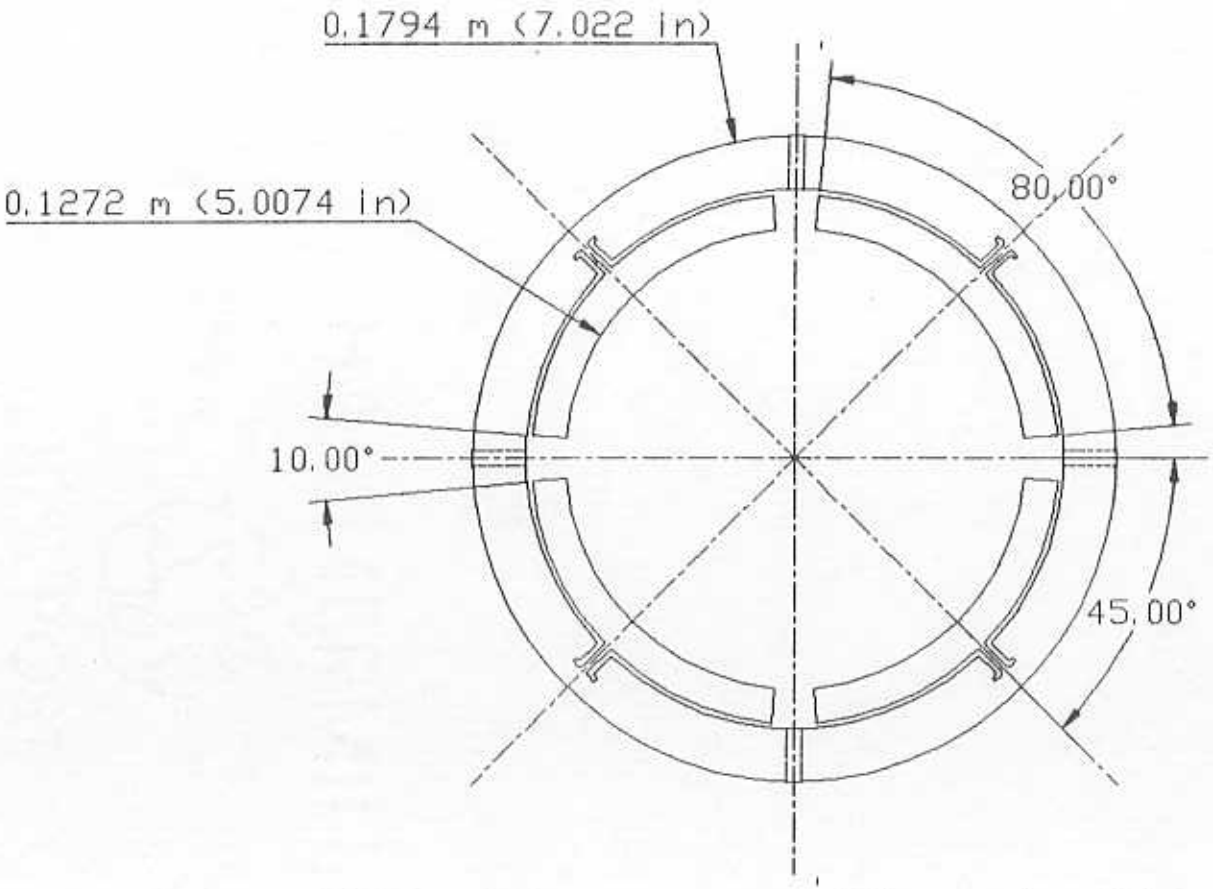

Figure 30. KMC Flexure Pivot Tilt Pad Bearing

Note: T* Indicates the postion of the * thermocouple.

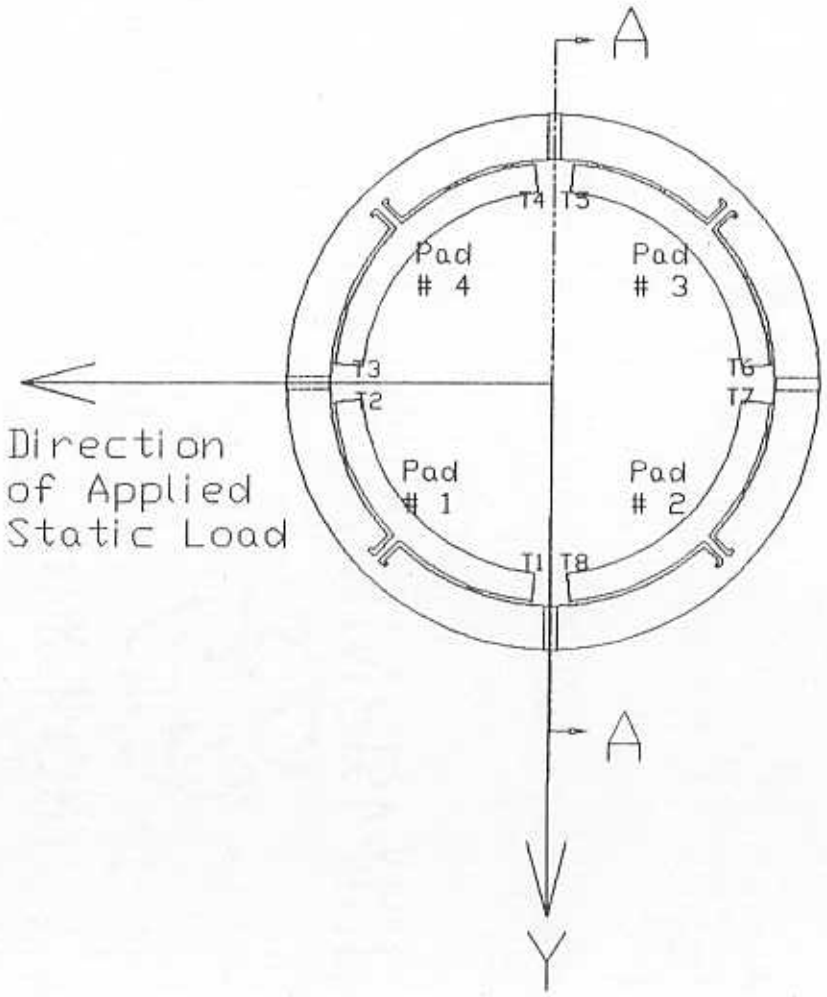

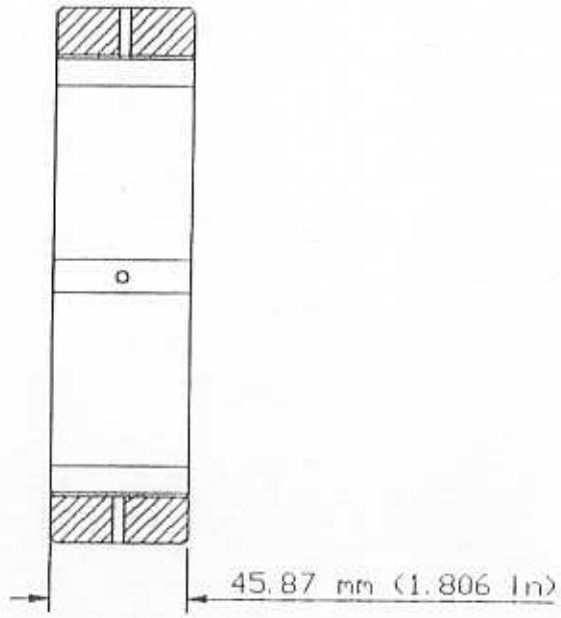

Section A-A

Figure 31. Setup Description

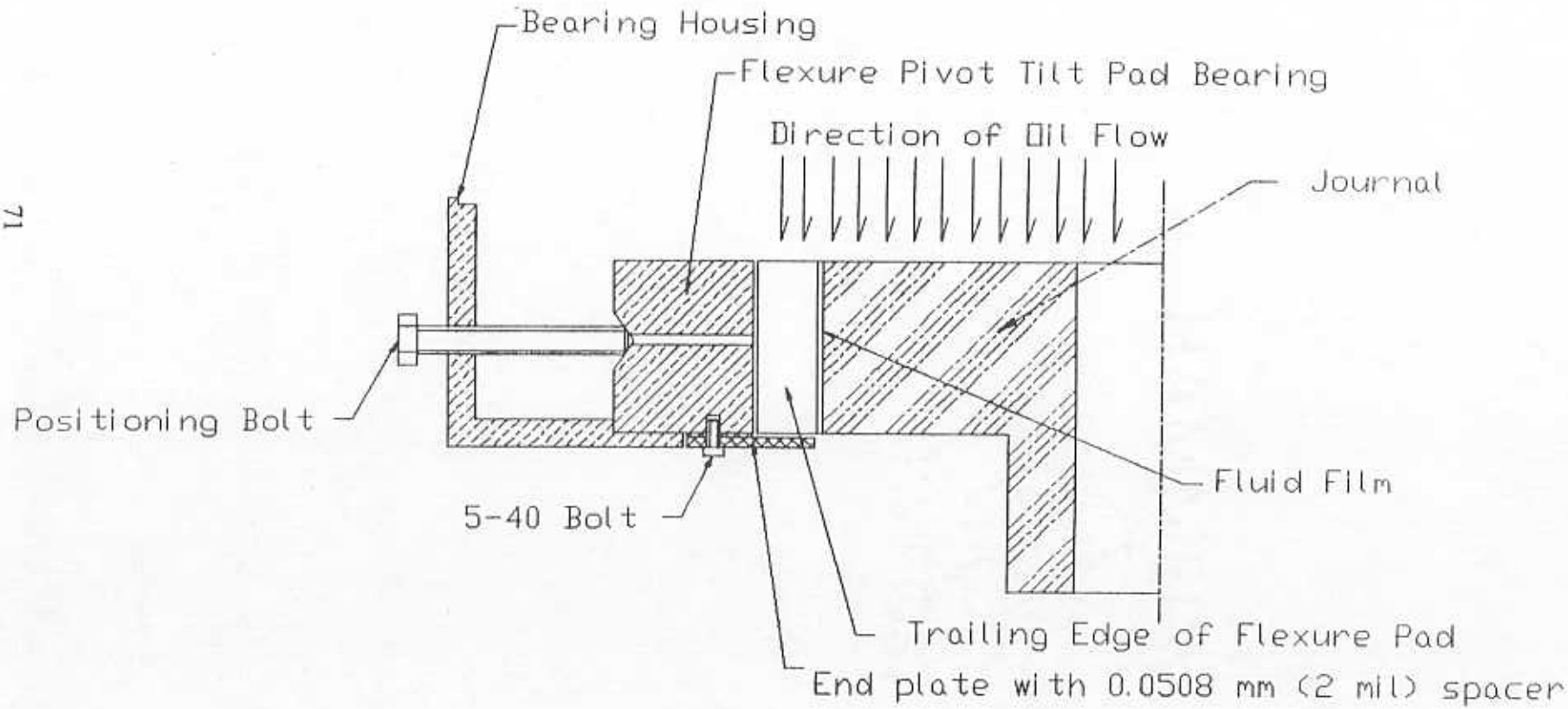

Figure 32: Test Bearing Modifications - End Plates

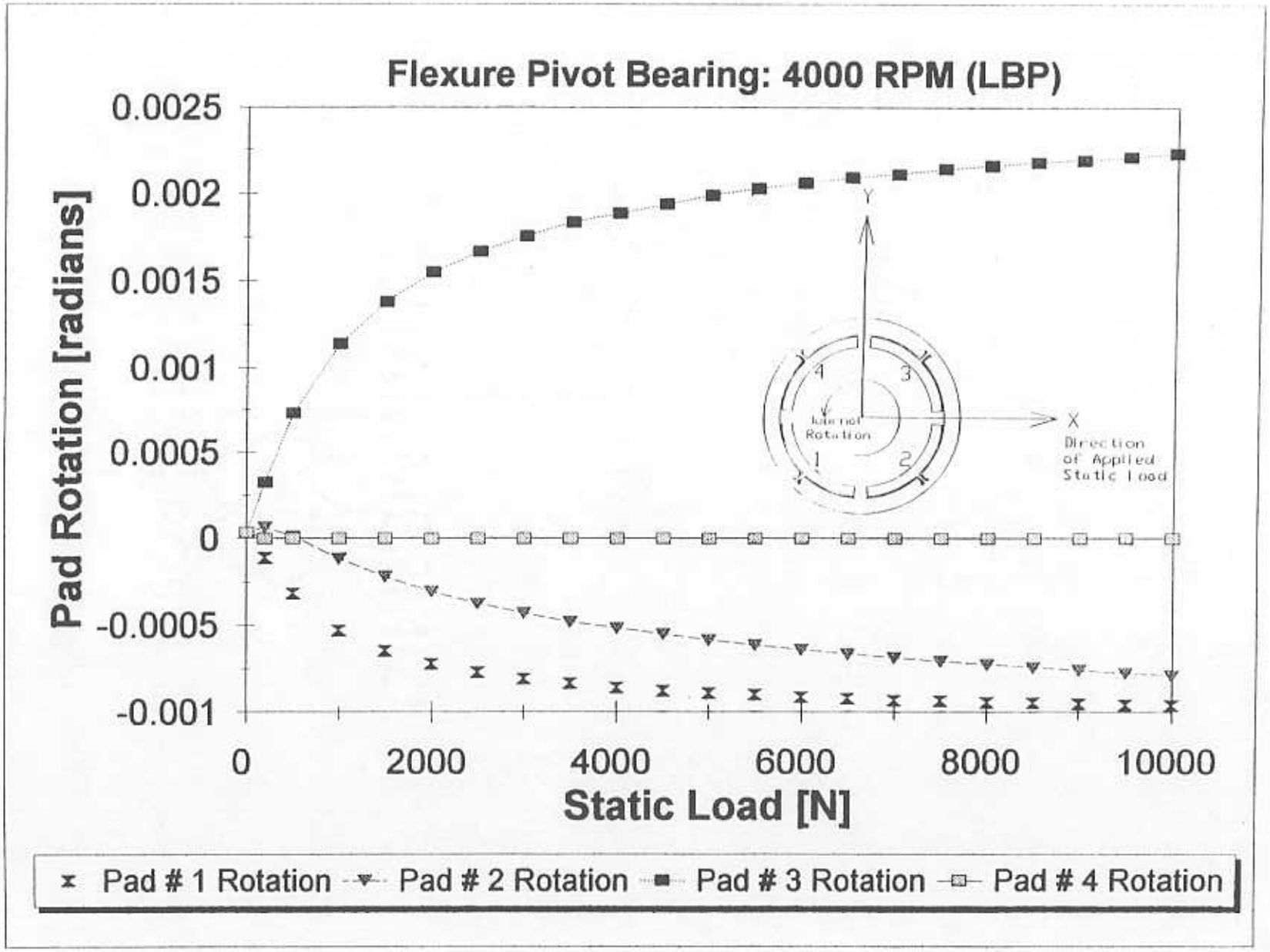

Figure 33: Prediction of pad rotations for applied load between pads

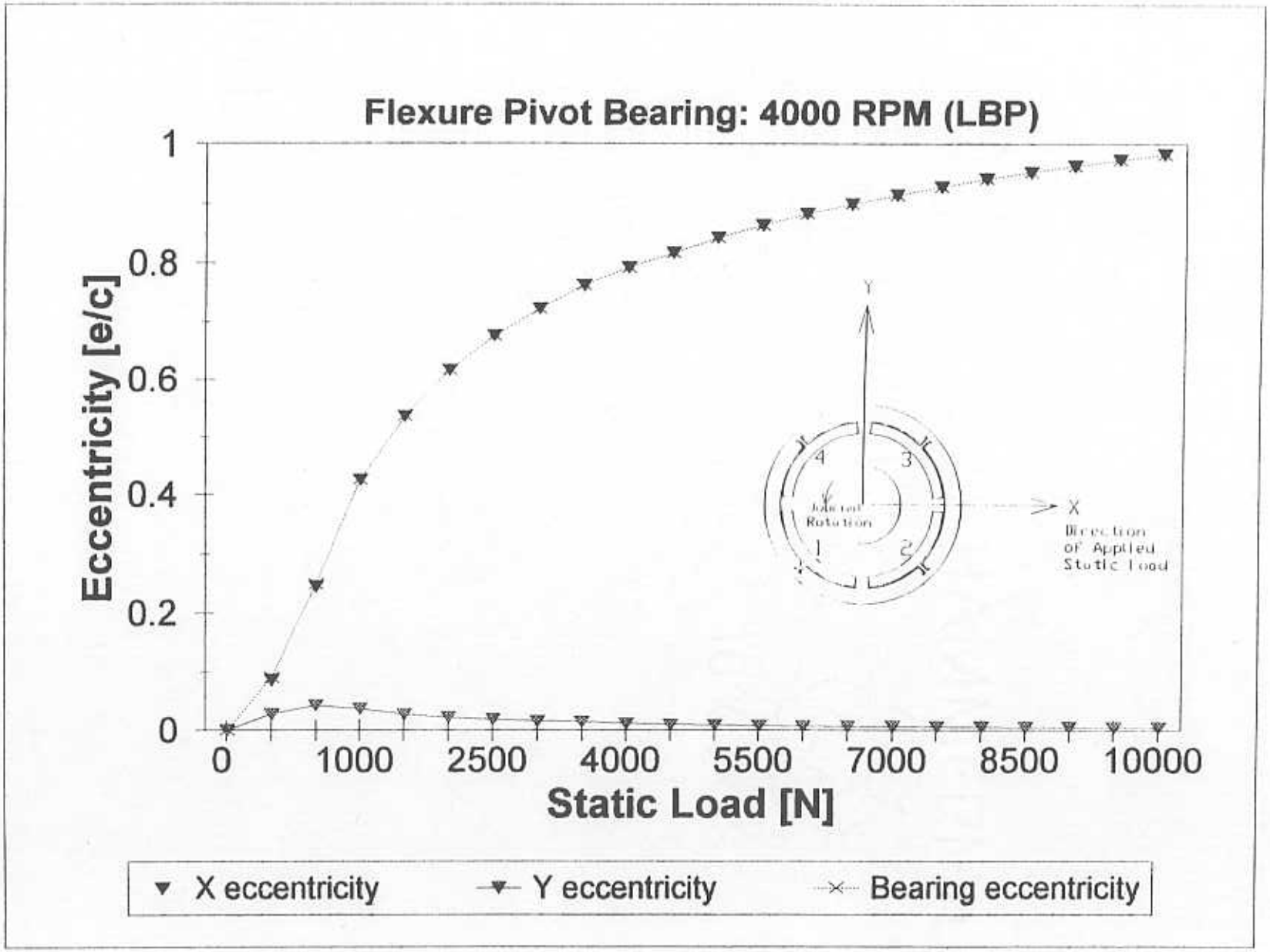

Figure 34: Prediction of operating eccentricity for applied load between pads

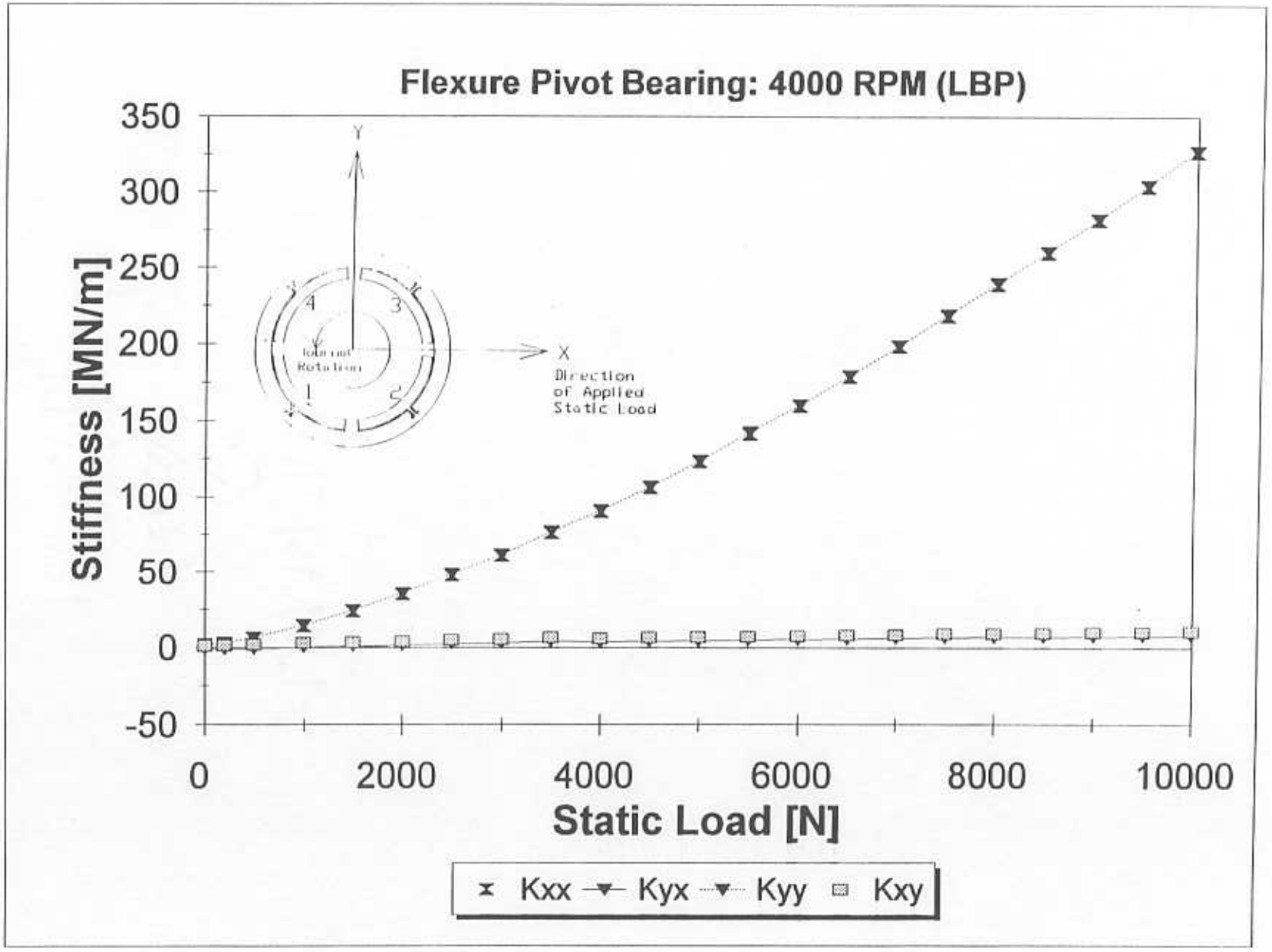

Figure 35: Synchronously Reduced Stiffness Cofficients for applied load between pads

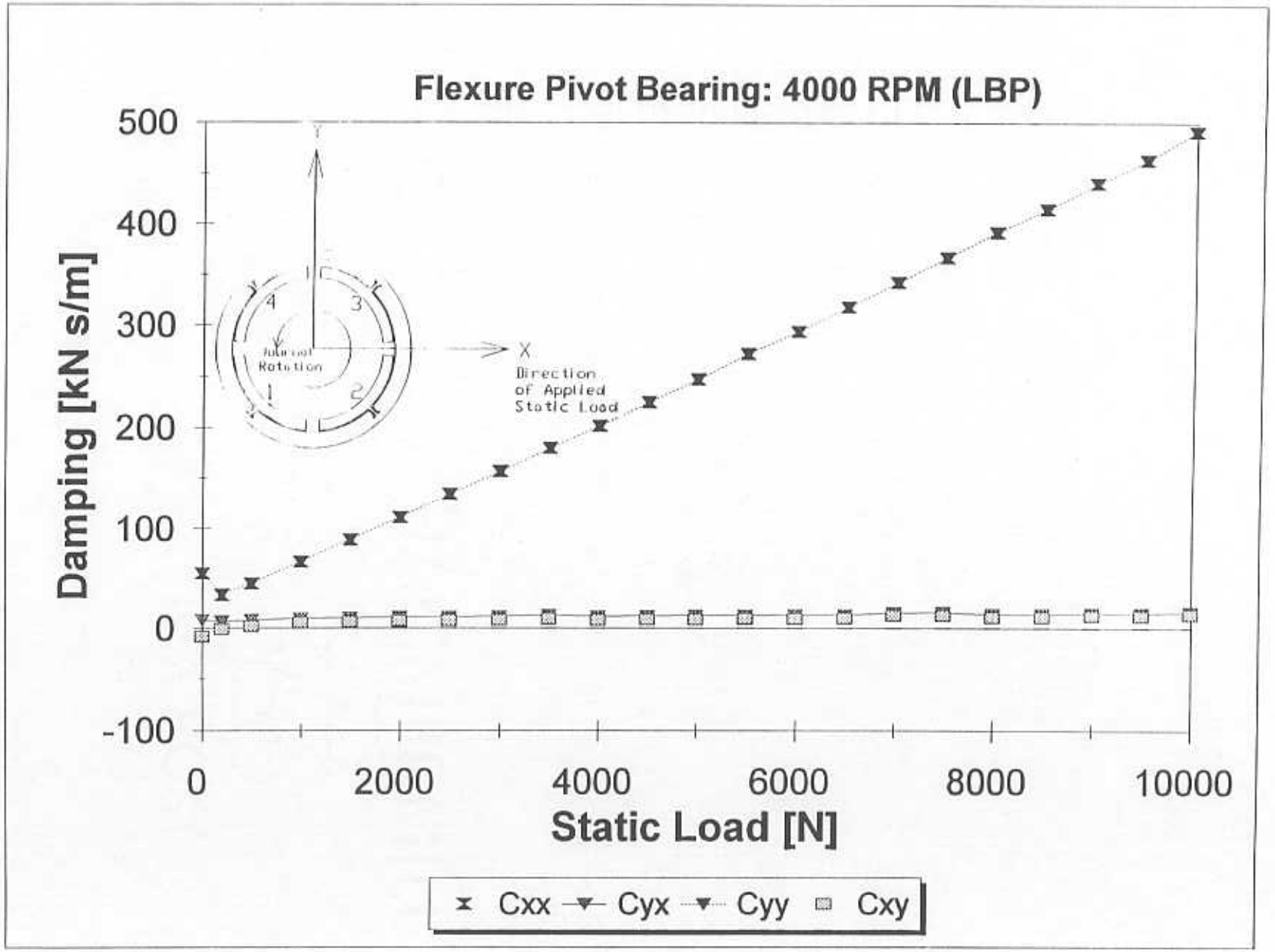

Figure 36: Synchronously Reduced Damping Cofficients for applied load between pads

REFERENCES - PART III.

Armentrout, R. W. and Paquette, D. J., 1993, "Rotordynamic Characteristics of Flexure-Pivot Tilting-Pad Journal Bearings," *STLE Tribology Transactions*, Vol. 36, pp. 443-451.

Arumugam, P., Swarnamani, S., and Prabhu, B. S., 1994, "Experimental Identification of Linearized Oil Film Coefficients of Cylindrical and Tilting Pad Bearings," ASME Paper 94-GT-81.

Chen, W. J., 1994, "Bearing Dynamic Coefficients of Flexible-Pad Journal Bearings," *Proc. of the ASME/STLE Tribology Conference, Lahaina, Hawaii*, Preprint 94-TC-4D-1.

De Choudhury, P., Hill, M. R., and Paquette, D. J., 1992, "A Flexible Pad Bearing System for a High Speed Centrifugal Compressor," *Proc. Of the 21st Turbomachinery Symposium, Dallas, TX*, pp. 57-64.

De Choudhury, P. and Masters, D., 1983, "Performance Tests of Five-Shoe Tilting-Pad Journal Bearing," *ASLE Transactions*, Vol. 27, pp. 61-66.

Nicholas, J., 1994, "Tilting Pad Bearing Design", *Proc. of the 23rd Turbomachinery Symposium, Dallas, TX*, pp. 179-194.

Nicholas, J. C., Gunter, E. J., and Allaire, P. E., 1977, "Stiffness and Damping Coefficients for the Five-Pad Tilting-Pad Bearing," *ASLE Transactions*, Vol. 22, pp. 113-124.

Parkins, D. W., and Horner, D., 1992, "Tilting Pad Journal Bearings - Measured and Predicted Stiffness Coefficients," *Proc. of the ASME/STLE Tribology Conference, San Diego, California*, Preprint 92-TC-3D-2.

Parsell, J. K., Allaire, P. K., Barrett, L. E., 1982, "Frequency Effects in Tilting-Pad Journal Bearing Dynamic Coefficients," *ASLE Transactions*, Vol. 26, pp. 222-227.

San Andres, L. A., 1994, "hydroflext and hydrotran User's Manual," Mechanical Engineering Dept., Texas A&M University.

Zeidan, F. Y., 1992, "Developments in Fluid Film Technology," *Turbomachinery Intel*, Vol. 9, pp. 24-31.